N-18173

THE DEVELOPMENT OF AN EXPERIMENTAL TECHNIQUE FOR DETERMINING THE FORCES AND MOMENTS ON MODELS IN SPINNING ATTITUDES AND A STUDY OF RESULTS OBTAINED

A Thesis

Presented to

the Faculty of the Department of Engineering

University of Virginia

APR 1971
RECEIVED
NASA STI FACILITY
INPUT BRANCH

In Partial Fulfillment

of the Requirements for the Degree

Master of Science in Aeronautical Engineering

by

Ralph W. Stone, Jr.

March 1952

FACILITY FORM 602

N71-72239 (ACCESSION NUMBER) (THRU)

112 (PAGES) None (CODE)

TMX-67010 (NASA CR OR TMX OR AD NUMBER) (CATEGORY)

THE DEVELOPMENT OF AN EXPERIMENTAL TECHNIQUE FOR DETERMINING THE FORCES AND MOMENTS ON MODELS IN SPINNING ATTITUDES AND A STUDY OF RESULTS OBTAINED

A Thesis

Presented to

the Faculty of the Department of Engineering

University of Virginia

In Partial Fulfillment

of the Requirements for the Degree

Master of Science in Aeronautical Engineering

---

by

Ralph W. Stone, Jr.

March 1952

APPROVAL SHEET

A thesis presented to the faculty of the Department of Engineering, University of Virginia, in partial fulfillment of the requirements for the Degree Master of Aeronautical Engineering.

Author - Ralph W. Stone Jr.

Faculty Advisor - Charles J Donlon

Subcommittee on Graduate Studies - Thomas W Williams

ACKNOWLEDGMENTS

The author is indebted to Messrs. A. I. Neihouse and C. H. Zimmerman of the Langley Aeronautical Laboratory for guidance and inspiration in the development of the rotary balance, the device presented and discussed herein, and in a thorough understanding of the data obtained.

TABLE OF CONTENTS

PAGE

INTRODUCTION 1

GENERAL CONSIDERATIONS 3

EXPERIMENTAL APPARATUS 5

The rotary balance 5

The free-spinning tunnel 9

DESIGN, CONSTRUCTION, AND PREPARATION OF MODELS 10

TESTING TECHNIQUES AND PROCEDURES 12

TESTS AND MEASUREMENTS 14

CORRECTIONS AND ACCURACY 17

PRESENTATION OF RESULTS 20

DISCUSSION OF RESULTS 22

General Aerodynamic Characteristics in Spins 22

Relation of the Aerodynamic Characteristics to the Inertia Characteristics in Spins 24

Effect of Rudder Reversal on Aerodynamic Coefficients 30

Total Aerodynamic Yawing Moment Required to Obtain Satisfactory Spin Recovery 32

Effect of Horizontal-Tail Position on Aerodynamic Coefficients and Rudder-Reversal Effectiveness 36

Effects of Lowering Landing Gear and Deflecting Flaps on Spin Attitudes and Aerodynamic Coefficients 38

CONCLUSIONS 39

REFERENCES 42

PAGE

APPENDIX 44

APPENDIX A 44

APPENDIX B 52

TABULATED RESULTS 59

FIGURES 69

LIST OF TABLES

TABLE		PAGE
I.	Corresponding Full-Scale Dimensional Characteristics of a Fighter Model	59
II.	Corresponding Full-Scale Mass Characteristics of a Fighter Model	60
III.	Free-Spinning Characteristics of 1/20-Scale Model and Aerodynamic Force and Moment Coefficients of 1/10-Scale Model of a Fighter Airplane in Spins	61
IV.	Tail-Damping Power Factors for the Various Tail Configurations Tested on a Fighter Model	62
V.	Comparison of Approximate Spin Radii and Sideslip Angles Tested and Spin Radii and Sideslip Angles Calculated from Measured Aerodynamic Forces	63
VI.	The Effect of Rudder Reversal on the Number of Turns for Recovery and on the Aerodynamic Force and Moment Coefficients of a Fighter Model in a Spin	64
VII.	The Effect of Unshielding the Vertical Tail by Horizontal-Tail Movement on the Aerodynamic Force and Moment Coefficients of a Fighter Model in a Spin	65
VIII.	The Effect of Unshielding the Vertical Tail on Rudder-Reversal Effectiveness on a Fighter Model in a Spin	66

TABLE PAGE

IX. Effect of Landing Flaps on the Yawing-Moment-Coefficient Increments Due to Setting the Rudder from Full With to Full Against the Spin on a Fighter Model 67

X. Comparison of the Resultant Inertia and Aerodynamic Force Coefficients and of the Inertia and Aerodynamic Moment Coefficients of a Fighter Model in a Spin 68

LIST OF FIGURES

Illustrations

FIGURE		PAGE
1.	Illustration of an Airplane in a Steady Spin. Arrows Indicate Positive Directions of Forces and Moments along and about the Body Axes of the Airplane	69
3.	The Rotary Balance in the Langley 20-Foot Free-Spinning Tunnel	71
4.	Illustration of the Six-Component Strain-Gage Balance . .	72
6.	Drawing of the 1/10-Scale Model of a Fighter Airplane as Tested on the Rotary Balance. Wing Incidence 2-1/2° Leading Edge Up; Stabilizer Incidence 1° Leading Edge Up. Center-of-Gravity Position Shown for Normal Loading	74
12.	Original and Modified Longitudinal Positions of Horizontal Tail Tested on the 1/20-Scale and 1/10-Scale Models of a Fighter Airplane. Dimensions are Full Scale	80
13.	Original Location of the Horizontal Tail Tested and the Antispin Fillets Tested on the 1/20-Scale and 1/10-Scale Models of a Fighter Airplane. Dimensions are Full Scale	81
14.	Modifications to the Vertical Tail Tested on the 1/20-Scale and 1/10-Scale Models of a Fighter Airplane. Dimensions are Full Scale	82

FIGURE PAGE

15. Ventral Fins Tested on the 1/20-Scale and 1/10-Scale Models of a Fighter Airplane. Dimensions are Full Scale 83

20. Illustration of Several Systems of Axes with Relation to a Spinning Airplane. Body, Wind, and Earth Axes are Shown 88

Photographs

2. The Spinning Model is Supported in the Tunnel by the Vertically Rising Air Current and the Character of the Spin is Recorded by Means of Motion Pictures. One of the Three Operators Launches the Model into the Tunnel, a Second Operator Controls the Airspeed and the Third Operates the Camera 70

5. The Instrument Panel of the Rotary Balance System for Recording the Force and Moment Data 73

7. The 1/10-Scale Model of a Fighter Airplane in the Clean Condition 75

8. The 1/10-Scale Model of a Fighter Airplane in the Landing Condition and with External Wing Fuel Tanks Installed . . 76

9. The 1/20-Scale Model of a Fighter Airplane in the Clean Condition 77

10. The 1/10-Scale Model of a Fighter Airplane Mounted on the Rotary Balance in the Langley 20-Foot Free-Spinning Tunnel 78

FIGURE PAGE

11. Photograph of the 1/20-Scale Model of a Fighter Airplane Spinning in the Langley 20-Foot Free-Spinning Tunnel . . 79

16. Moment-of-Inertia and Center-of-Gravity Gear 84

(a) Moment-of-inertia gear 84

(b) Center-of-gravity gear 84

Graphs

17. Variation of the Increment of Yawing-Moment Coefficient Caused by Rudder Reversal with Angle of Attack for Spin of a Model of a Fighter Airplane. Numbers Refer to Test Conditions in Table III 85

18. Variation of Yawing-Moment Coefficient Caused by Setting the Rudder against the Spin with Angle of Attack for Spins of a Model of a Fighter Airplane. Numbers Refer to Test Conditions in Table III 86

19. Effect of Horizontal-Tail Position on the Increment of Yawing-Moment Coefficient Caused by Rudder Reversal for Spins of a Model of a Fighter Airplane. Numbers Refer to Test Conditions in Table III 87

DEFINITION OF COEFFICIENTS AND SYMBOLS

The rotary balance was designed to measure forces and moments with respect to the body axis. A diagram of these axes showing the positive direction of the forces and moments is presented in Figure 1. The coefficients and symbols used in this paper are generally in relation to these body axes and are listed herewith.

C_X longitudinal-force coefficient $\left(\frac{X}{\frac{1}{2}\rho V^2 S}\right)$

C_Y lateral-force coefficient $\left(\frac{Y}{\frac{1}{2}\rho V^2 S}\right)$

C_Z normal-force coefficient $\left(\frac{Z}{\frac{1}{2}\rho V^2 S}\right)$

C_R resultant-force coefficient

C_l rolling-moment coefficient $\left(\frac{L}{\frac{1}{2}\rho V^2 bS}\right)$

C_m pitching-moment coefficient based on wing span $\left(\frac{M}{\frac{1}{2}\rho V^2 bS}\right)$

C_n yawing-moment coefficient $\left(\frac{N}{\frac{1}{2}\rho V^2 bS}\right)$

X longitudinal force acting along X body axis, positive forward, pounds

Y lateral force acting along Y body axis, positive to right, pounds

Z normal force acting along Z body axis, positive downward, pounds

L rolling moment acting about X body axis, positive when it tends to lower right wing, foot-pounds

M	pitching moment acting about Y body axis, positive when it tends to increase the angle of attack, foot-pounds
N	yawing moment acting about Z body axis, positive when it tends to turn airplane to right, foot-pounds
p	rolling angular velocity about X body axis, radians per second
q	pitching angular velocity about Y body axis, radians per second
r	yawing angular velocity about Z body axis, radians per second
$\frac{dp}{dt}$	rate of change of rolling angular velocity with time
$\frac{dq}{dt}$	rate of change of pitching angular velocity with time
$\frac{dr}{dt}$	rate of change of yawing angular velocity with time
Ω	full-scale angular velocity about spin axis, radians per second unless otherwise indicated
$\Omega b/2V$	spin coefficient
S	wing area, square feet
b	wing span, feet
ρ	air density, slugs per cubic foot
V	free-stream velocity in balance tests, or full-scale true rate of descent in free-spinning tests, feet per second
$\bar{c}$	mean aerodynamic chord, feet
c	local chord, feet
R_s	spin radius, distance from spin axis to center of gravity, feet

$x/\bar{c}$	ratio of distance of center of gravity rearward of leading edge of mean aerodynamic chord to mean aerodynamic chord
$z/\bar{c}$	ratio of distance between center of gravity and thrust line to mean aerodynamic chord (positive when center of gravity is below thrust line)
W	weight of airplane, pounds
g	acceleration due to gravity, 32.2 feet per second per second
m	mass of airplane, slugs (W/g)
μ	airplane relative-density coefficient ($m/\rho Sb$)
I_X, I_Y, I_Z	moments of inertia about X, Y, and Z body axes, respectively, slug-feet^2
$\frac{I_X - I_Y}{mb^2}$	inertia yawing-moment parameter
$\frac{I_Y - I_Z}{mb^2}$	inertia rolling-moment parameter
$\frac{I_Z - I_X}{mb^2}$	inertia pitching-moment parameter
α	angle between vertical and X body axis (approximately equal to absolute value of angle of attack at plane of symmetry), degrees
ϕ	angle between span axis and horizontal, positive when right wing is down, degrees
Ψ	angle between projection of resultant-force vector and projection of Z body axis in a horizontal plane, degrees

β_{cg} approximate angle of sideslip at center of gravity (angle between relative wind and plane of symmetry at center of gravity), positive when relative wind comes from right of plane of symmetry, degrees

β_t approximate angle of sideslip at tail (angle between relative wind and plane of symmetry at tail), positive when relative wind comes from right of plane of symmetry, degrees

INTRODUCTION

The spinning and spin recovery of airplanes, from the outset of man's ability to fly, have been subjects of concern to designers and pilots. The spin is a motion, frequently entered inadvertently, in which the airplane descends toward the earth along the path of a helix with the nose of the airplane generally pointing well below the horizon. In this motion, the airplane is at an angle of attack which is greater than the angle of attack at which the airplane's maximum lift coefficient is obtained. The spin is entered because the angle of attack of maximum lift is exceeded by the pilot. The motion is generally considered uncontrollable in that the airplane does not respond to control movement in the normal manner and if the airplane is not properly designed, recovery from the spinning motion is difficult and sometimes impossible.

Analytical treatment of the spin and spin-recovery problem has not proved to be an adequate solution, primarily because of the complicity of the spinning motions and its equations which involve six degrees of freedom, and which generally have variable coefficients. Further there is practically a complete lack of knowledge as to what the aerodynamic coefficients and derivatives are for spinning attitudes. Basic studies of the spin were made by the British (References 1 and 2) which generally indicate the complicity of the motion and its analytical treatment.

The experimental method of solution of the spin problem has been used extensively. The NACA free-spinning tunnels (Reference 3) have given relatively rapid solutions to the spin and spin-recovery problems

of specific designs by the use of visually observed and recorded spin and recovery characteristics of models of these designs. The results of these free-spinning investigations had led to empirical criterions (References 4, 5, and 6) based on the general geometric and mass characteristics of numerous designs investigated in the NACA free-spinning tunnels. New airplanes with similar geometric and mass characteristics to those previously investigated may be designed with reasonable assurance that they will have satisfactory spin-recovery characteristics by use of these criteria.

It was realized in the past that the effects of the various components of an airplane on the spin and spin recovery could be determined by measurements of the aerodynamic forces and moments exerted on a spinning airplane. It also has been realized more recently that such measurements would be desirable to improve existing criteria and to obtain a broader understanding of the spin and spin recovery. Early measurements were made on small models of rotating wings and airplanes by the use of an intricate spinning balance in the NACA 5-foot vertical wind tunnel (References 7 to 15). Work with this original balance was discontinued because of lack of reliability and the exceeding difficulty of operation involved in the test procedure. The results of these investigations, also, were not considered sufficiently extensive for or applicable to airplane of current and expected designs. Because of these factors and because the need for force and moment measurement on models at spinning angles of attack was becoming eminently important, a new balance, much simpler and more

reliable than the original spinning balance was needed. The author undertook the general design, construction, and installation of such a balance which would measure the forces and moments of rotating models at spinning angles of attack. The present paper presents briefly the development of this rotary balance and a study of the initial results obtained.

GENERAL CONSIDERATIONS

The steady spin is essentially a rotation of an airplane about a vertical axis with the center of gravity at some fixed radius from the vertical axis and the angle of attack larger than the stalling angle of attack. The rotation is constant and the rate of descent is constant, such that the center of gravity describes a helical path about the vertical axis, as is shown in Figure 1. In the spin tunnel, such spins are studied by having a geometrically and dynamically scaled model launched into a vertically rising air stream. The velocity of this air stream is adjusted until it equals the rate of descent of the model and thus the spin is studied. In the case of free models, such as a spinning model, where gravity has considerable influence in the motion, the primary similarity rule which must be considered is the Froude number. The relationships regarding the similarity between free models and airplanes, based fundamentally on Froude number, are given in Appendix A.

In designing a rotary balance to measure the forces and moments which act in spins, it was necessary to duplicate the motion of the free

model or airplane as nearly as possible with a model supported in such a manner that the forces and moments may be measured and transferred to appropriate recording devices. It was necessary, therefore, to have an axis of rotation about which the model rotates with the proper radius, angle of attack, angle of sideslip, and orientation of the model axis with relation to the axis of rotation. Also a velocity must be superimposed on the system, this velocity being parallel to axis of rotation.

Dynamic similitude implies primarily that the path of motion of a model, subjected to the rules of similarity of Appendix A, is geometrically similar to that of the airplane which the model represents. The model on the rotary balance also should perform a geometrically similar path to that of the airplane. Each part of the model, the center of gravity, the tail, the wing tips, etc., must perform the similar paths. This implies that $\frac{\Omega R}{V}$ and the orientation angles α and ϕ must be identical for the model and the airplane it represents. The specific relations presented in Appendix A, such as the relations for velocity (V), rate of rotation (Ω), etc., do not necessarily have to be obtained on the rotary balance model. It is only necessary to satisfy the relation $\frac{\Omega R}{V}$ and the other attitude relation previously mentioned.

With these factors under consideration, the rotary balance was developed to be installed in the NACA 20-foot spin tunnel. A detailed description of the rotary balance is given in a later section of this paper. The basic balance was made of a system of strain gages because

of their compactness and because information measured by strain gages could be transmitted relatively easily, from the rotating model, with the strain-gage balance contained internally, to stationary recorders through a system of slip rings. Other measuring and recording systems are not as readily adaptable. A detailed description of the strain-gage balance used with the rotary balance is given in a later section of this paper.

The rotary balance was not developed to replace the free-spinning tunnel technique but more to supplement it. The free-spinning tunnel has proved a rapid and efficient method of determining the spin and recovery characteristics of specific airplanes. In its supplementary roll, it is intended that the rotary balance give deeper insight to the mechanisms of the spin and recovery by giving a more complete knowledge of the forces and moments acting. It is also intended that rotary balance results will eventually improve existing empirical criterions (References 4, 5, and 6) by relating them to conventional aerodynamic coefficients such as yawing-moment coefficient C_n. The approximate magnitudes of the control moments, due to rudder, elevator or aileron reversal, required may also be obtained in the future.

EXPERIMENTAL APPARATUS

The rotary balance. The rotary balance used for the measurements of aerodynamic forces and moments on rotating models was designed for use in the 20-foot free-spinning tunnel as has been previously noted. The size model for which the balance was designed was about twice the

size of free-spinning models or about 5 feet in span. It was felt that this size model was relatively small with relation to the tunnel diameter (20 feet) so that interference effects would be negligible but that it was sufficiently large to obtain readily satisfactory balance results. The rotary balance consists essentially of two major parts, the six-component balance itself and the operating mechanism used to mount the model and balance and to rotate them in the tunnel. A schematic diagram of the entire rotary balance system as installed in the tunnel is shown in Figure 3. Because the rotary balance was to be used in the 20-foot free-spinning tunnel, the primary purpose of which was to perform free dynamic tests, it was necessary to design the balance system in such a manner that it could be readily removed from the tunnel or moved to a position out of the way of free-spinning models. Toward this end the main horizontal supporting arm (part G in Figure 3) was hinged on a vertical axis so that the balance could be rotated from the center of the tunnel to the tunnel wall, there being out of the way of free-spinning models and, further, accessible to the test section doors of the tunnel for installation and adjustment of the models on the balance and for ease of maintenance of the balance system. In addition to the horizontal supporting arm, the rotary balance system consists of cables (part F) and winches which move the supporting arm as noted above. The rotary arm of the balance system (part A), which rotates about a vertical axis, is attached at the outer end of the horizontal supporting arm and is driven by a dive shaft (part D) and appropriate linkages. The drive shaft is turned by

an electric motor and a Graham friction drive by which the rate of rotation may be varied up to 200 rpm in either direction. Adjustable counter weights (part E) are attached to the upper end of the rotary arm to counterbalance other rotating parts. At the lower end of the rotary arm is a spin-radius setting arm (part H) that can be adjusted to simulate various radii from the center of rotation. At the end of the spin-radius setting arm is the model-attitude setting block (part F) to which the actual balance (part J) and model are attached. This block can be adjusted so as to simulate various angles of attack and sideslip of the model. The range of angles of attack and sideslip may be varied from 0° to 360°.

The actual balance consists of a six-component strain gage that measures normal, longitudinal, and lateral forces and rolling, pitching, and yawing moments about the body axes. The strain-gage balance is a small compact unit, as illustrated in Figure 4, consisting of 12 strain-gage beams, two beams for each of the six components it measures. Storage batteries provide the direct current for the strain-gage balance system, and the voltage is measured and regulated at a control panel (Figure 5). The current from the storage batteries is transmitted to the rotating strain gages through a system of brushes and slip rings (part C, Figure 3) that are mounted above the rotary arm (Figure 3). Each pair of strain-gage beams is wired into a Wheatstone bridge circuit that is electrically balanced when no external loads are present. When an external load is applied, the strain-gage beams are deflected changing the resistance of the strain gages and, consequently,

the bridge is unbalanced. The current flow resulting from the unbalanced bridge is transmitted back through the slip-ring-brush arrangement where it is measured on a calibrated microammeter.

Six microammeters (one for each force and moment to be measured) are mounted in the instrument panel shown in Figure 5. Also included on this panel are a voltmeter for maintaining proper voltage in the Wheatstone bridge systems, a rate-of-rotation regulator and indicator, and a tunnel airspeed control. A micromanometer is also included from which the tunnel airspeed may be determined.

In order to determine the design requirements for the rotary balance system and the strain gages, the free-spinning results of nearly 200 different designs were studied. The ranges of attitudes, rates of rotation, spin radii, and vertical velocities which might be required by the rotary balance were determined. Calculations of the inertia moments and forces of some of the 200 designs also were made to estimate the ranges of longitudinal, normal, and lateral forces; and of the pitching, rolling, and yawing moments which the strain-gage balance was expected to be subjected. Calculations of the expected moments were made by the use of Euler's dynamical equations of motions of rigid bodies. It is assumed that models in spins are rigid dynamic bodies and no consideration of aeroelastic effects have been made. The inertia or mass forces considered in the analysis were the weight and the centrifugal forces of the rotating models. From the results of these studies, with consideration of the

differences in size of the free-spinning model studies and those which were expected to be used on the rotary balance, the normal-force, longitudinal-force, and lateral-force beams were designed to take 26, 15, and 4 pounds, respectively. The rolling-, pitching-, and yawing-moment beams were designed to take 15, 12, and 8 foot-pounds, respectively.

The free-spinning tunnel. The free-spinning results presented herein and the results used for the development of the spin criterions, presented in References 4, 5, and 6, were obtained in the NACA 20-foot free-spinning tunnel. The 20-foot free-spinning tunnel, presently in operation, is similar in design and operation to the original NACA 15-foot free-spinning tunnel described in Reference 3. The 20-foot tunnel is, in brief, a vertical wind tunnel in which the air is drawn vertically upward through the test section by a propeller and power unit at the top of the tunnel. The tunnel proper is a 12-sided structure 20 feet across the flats at the test section. The tunnel is capable of airspeeds of from 0 to approximately 100 feet per second at the test section and requires about 1200 horsepower at top speed. For free-spinning tests, models are launched by hand into the vertically rising air stream, with an imposed spinning motion. The tunnel operator adjusts the airspeed such that the velocity of the vertically rising air stream is equal to the rate of descent of the model as has been previously noted. Thus, the model is sustained in a spin at a fixed level in the tunnel and is there observed and photographed by a motion-picture camera. A general view of the tunnel showing these operations

is presented in Figure 2. The models when launched into the tunnel have their controls set into the positions desired to be investigated. After the steady spin or the motion associated with the given control positions is recorded, recoveries from these motions are attempted. Recoveries are attempted by movement of one or more of the various controls by use of a remote-control mechanism. This mechanism consists primarily of an electromagnet, batteries, a magnetic switch, and a triggering system. The heart of the mechanism is the magnetic switch which consists of two permalloy strips which are attracted to one another in the presence of magnetism. When the magnetic switch is operated, a circuit is closed energizing the electromagnet which operates the trigger mechanism and thus moves the desired controls. The magnetic field used to operate the magnetic switch is created by the use of copper bar windings around the perimeter of the test section. The windings are energized, at will, by the operator. At the completion of a given test, the model is retrieved from the tunnel by use of retrieving pole and clamp.

DESIGN, CONSTRUCTION, AND PREPARATION OF MODELS

The free-spinning tunnel tests presented herein were performed on a 1/20-scale model of a fighter airplane. The force and moment measurements made on the rotary balance were made on a 1/10-scale model of the same fighter airplane. This model was exactly scaled up from the 1/20-scale dynamic model. A three-view drawing of the 1/10-scale model in its original configuration, with flaps and landing gear

retracted and the cockpit closed, is shown in Figure 6. The full-scale dimensional characteristics of the fighter airplane simulated by the models are given in Table I and the full-scale mass characteristics simulated on the models are given in Table II. Figure 7 is a photograph of the 1/10-scale model in the clean condition and Figure 8 shows the 1/10-scale model in the landing condition and in the condition with external fuel tanks installed. The 1/20-scale model in the clean condition is shown in Figure 9. A photograph of the 1/10-scale model mounted on the rotary balance is shown in Figure 10. A photograph of the 1/20-scale model spinning in the 20-foot free-spinning tunnel is shown as Figure 11.

The dynamic 1/20-scale model was built primarily of balsa with some hard wood for structural strength. The remote-control mechanism, previously discussed, was installed in the model and all control surfaces were made movable such that they could be set at any desired position or moved from any preset position to any other position by the remote-control mechanism.

The 1/10-scale balance model was of built-up construction with plywood bulkheads and ribs planked with balsa strips. On this model too, the controls were made movable so that they could be set at any desired position.

Landing gear, landing flaps, and external fuel tanks were constructed for use on each model. In addition, each model was tested with the several tail modifications shown in Figures 12 to 15.

TESTING TECHNIQUES AND PROCEDURES

As has previously been stated, the 1/20-scale model was tested freely in the 20-foot free-spinning tunnel, the general operation of which has been discussed. The recoveries presented herein were attempted generally by rapid full rudder reversal. A recovery is considered satisfactory if the model stops spinning in 2-1/4 turns or less (Reference 4). This value has been selected on the basis of full-scale airplane spin-recovery data that have been available for comparison with corresponding model test results. The results of this comparison are presented in Reference 21.

The weight and moments of inertia of the airplane were scaled down from the values listed on Table II by the relationships developed in Appendix A. The model was ballasted to these scaled down values by the use of lead weight placed at convenient locations in the model. The center-of-gravity position and moments of inertia of the models were measured by the apparatus shown in Figure 16. The center-of-gravity gear is a simple beam balance from which the distance of the model's center of gravity from the knife edges of the balance is measured. The moment-of-inertia gear is a torsional pendulum upon which the model is oscillated about each of the various axis. The moments of inertia are proportional to the period of oscillations of the pendulum. The moments of inertia measured are termed virtual moments of inertia in that they include ambient air effects and the effects of the air entrapped within the model. The true moments of

inertia are obtained by correcting the virtual moments of inertia in accordance with Reference 22.

The 1/10-scale balance model as has previously been noted was mounted on the rotary balance in the 20-foot free-spinning tunnel for the tests reported herein. The model was set at attitudes and with control settings corresponding to those for the spins obtained with the 1/20-scale free-spinning model for the various conditions tested on this model. The 1/20-scale model had oscillated slightly in pitch, roll, and yaw while spinning and the average values of α and ϕ were used in setting the attitude of the 1/10-scale model.

The 1/10-scale model was mounted on the rotary balance in such a manner that the Z body axis of the model passed through the spin axis, although in an actual fully developed spin, as obtained with the 1/20-scale model, the resultant aerodynamic force vector passes through the spin axis. The Z axis of the model and the resultant aerodynamic force vector are not exactly coincident although as a first approximation it has been assumed to be a reasonable assumption.

The spin radii set on the 1/10-scale model were calculated from the data measured for the free-spinning model by the approximate formula

$$R_s = \frac{g \cot \alpha}{\Omega^2} \qquad (1)$$

The radii so calculated are only approximate in that the formula is based on the assumption made that the resultant force lies along the

Z body axis. The components of the resultant force are the weight and the centrifugal force, and the Z axis makes an angle α with the horizontal. Thus

$$mR_s\Omega^2 = mg \cot \alpha$$

and R_s is as noted in Equation (1).

The angular velocity about the spin axis and the rate of descent of the model observed in the free-spinning tests were used to calculate the spin coefficient $\Omega b/2V$. Preliminary tests of the model on the rotary balance indicated that at high rates of rotation vibrations of the rotary balance occurred and, accordingly, actual scale ratios of the higher rates of rotation as measured on the free-spinning model were not simulated. All tests were performed at the proper values of the spin coefficient $\Omega b/2V$, however. For simplicity, a constant tunnel velocity was used for all tests and was chosen so that the values of Ω required to obtain the proper values of the spin coefficient $\Omega b/2V$ were below that at which vibration started. A brief investigation made to determine the force and moment coefficients at a specific value of $\Omega b/2V$ but at different tunnel velocities indicated no noticeable effect within the range of velocities possible.

TESTS AND MEASUREMENTS

As has been previously mentioned, in order to check the validity of the results measured on the rotary balance, it was decided to compare these results with free-spinning model results. To accomplish this end, free-spinning model tests were first performed on the 1/20-scale model

of a fighter airplane. These results were then duplicated on the rotary balance as nearly as possible; that is, the attitude, spin radius, spin parameter, etc. obtained from free spins on the 1/20-scale model were set on the rotary balance with the 1/10-scale model. No concern was given to the differences in the Reynolds numbers between the two models. The Reynolds numbers of the tests on the 1/20-scale model were of the order of 200,000 whereas those for the 1/10-scale model were of the order of 400,000. Differences of this order of magnitude and in this range of values at angles of attack below the stall generally indicate little effect on the characteristics of airfoils. There are insufficient data at angles of attack above the stall and in the spinning range to ascertain the effects of Reynolds number in this angle-of-attack range. Trends of data at and just beyond the stall (Reference 16), however, indicate a diminishing effect of Reynolds number as angle of attack increases. It is felt, therefore, that the differences in Reynolds numbers between the free-spinning and rotary-balance tests are not significant for this investigation.

The spinning attitudes and spin coefficients for each of the various model conditions and control configurations tested on the 1/20-scale model are presented in Table III. The model was spun arbitrarily to the right for the tests presented herein because brief tests performed to the left had shown that the model had symmetrical spin and recovery characteristics. As previously mentioned, the mass characteristics and mass parameters for loadings tested on the model

are listed in Table II. Loadings 2 and 3 were obtained on the 1/20-scale dynamic model by installation of ballasted external fuel tanks. When the conditions for these loadings were tested on the 1/10-scale model, geometrically similar external tanks were installed.

The aerodynamic force and moment measurements on the 1/10-scale model were made for the same model conditions, control configurations, attitudes, and spin coefficients obtained on the 1/20-scale free-spinning model and presented in Table III.

The normal maximum control deflections used in the investigation were:

Rudder, degrees	±30
Elevator, degrees	±20
Ailerons, degrees	±14
Flaps, degrees	45

The intermediate control deflections used were:

Elevator two-thirds up, degrees	$-13\frac{2}{3}$
Ailerons two-thirds deflected, degrees	$\pm 9\frac{1}{3}$
Ailerons one-third deflected, degrees	$\pm 4\frac{2}{3}$

For the clean condition referred to herein, the cockpit was closed, the landing gear was retracted, and the flaps were neutral. For the landing condition, the flaps were deflected 45° and the landing gear was extended. Tests were also performed with the flaps deflected 45° and the landing gear retracted.

The modified tail configurations shown in Figures 12 to 15 were tested on the models. The tail-damping power factors (Reference 4) of the models for the various modifications are presented in Table IV.

As a result of the various model conditions, control configurations, and loadings, the investigation included large variations in spinning attitudes and spin coefficients, the angles of attack ranging from approximately 20° to 70°, the angles of sideslip at the center of gravity ranging from 3° inward to 7° outward, and spin coefficients $\Omega b/2V$ ranging from 0.16 to 0.38.

All balance tests were made at a tunnel airspeed of 68.5 feet per second, which gives an approximate Reynolds number of 420,000 based on the mean aerodynamic chord of the 1/10-scale model. This value of Reynolds number has not been corrected for the turbulence factor of the Langley 20-foot free-spinning tunnel, which is 1.8.

CORRECTIONS AND ACCURACY

The results of all wind-tunnel tests are considered in the light of the correctness with which the results actually represent the capabilities of the model. From this viewpoint, the following considerations were made of the data presented herein.

The forces and moments measured by the strain-gage balance were the sum of the aerodynamic forces and moments exerted on the 1/10-scale model and the centrifugal forces and inertia moments produced by the rotation of the model and strain-gage beams. The centrifugal-force and inertia-moment values produced by the rotating

model and strain-gage beams had to be subtracted from the values measured to obtain the aerodynamic values. In order to determine these corrections for each test, the centrifugal forces and inertia moments produced by the rotating model were calculated by using equations, presented in Reference 7, derived from Euler's dynamical equations. When these equations are used, the weight, center of gravity, and moments of inertia of the model must be known; therefore, these values were measured for the 1/10-scale model. The amounts of the centrifugal forces and inertia moments contributed by the strain-gage beams for each test were found experimentally.

Interaction of the forces and moments resulting from bending of the strain-gage beams when under load has been corrected for both in the measured aerodynamic characteristics and the calculated inertia tare corrections.

The effect of setting the 1/10-scale model on the rotary balance at a value of spin radius that was approximate was examined and its influence was considered in analyzing the results.

The tunnel-wall effects were not considered significant since the model was located a large distance from the tunnel wall and the span of the model was small with relation to the tunnel diameter. Consideration of the interference between the model and the rotary balance indicated that the model might have been in the wake of the balance only for steep spinning angles of attack. For these steep spinning angles of attack, the tail of the model may have been in the wake of the rotary-balance arm; but inasmuch as the tail was a large

distance behind the arm, where the wake disturbance was well-dissipated, no corrections were made for interference effects.

Because the 1/20-scale model was smaller than the 1/10-scale model and because it also was completely free in the tunnel, no significant corrections are felt to exist for the free-spinning case.

Consideration of the accuracy of the measurements made was also made by repeated testing and estimations of the accuracy of the actual measuring devices.

The free-spinning results presented herein are believed to be the true values given within the following limits:

α, degrees	± 1
ϕ, degrees	± 1
V, percent	± 5
Ω, percent	± 2
Turns for recovery, obtained from motion-picture records	$\pm 1/4$

The limits of accuracy of the measurements of the mass characteristics of both the 1/10- and 1/20-scale models are believed to be as follows:

Weight, percent	± 1
Center-of-gravity location, percent $\bar{c}$	± 1
Moments of inertia, percent	± 5

The limits of accuracy of the measurements of the electrical strain-gage system are estimated to be as follows:

C_X	±0.0082
C_Y	±0.0033
C_Z	±0.0127
C_l	±0.0007
C_m	±0.0011
C_n	±0.0004

The limits of accuracy of the increments of the coefficients are believed to be somewhat better than the values listed.

The spin conditions set on the rotary balance simulated those measured on the free-spinning model within the following limits:

α, degrees	±0.5
ϕ, degrees	±0.5
$\Omega b/2V$, percent	±1.5

PRESENTATION OF RESULTS

The results of the model investigations are presented generally in tabular form in that the free-spinning results and consequently the force and moment measurements do not result in systematic variations of what are normally considered in wind-tunnel work as independent variables. Because the spin is a free motion, it is not possible to vary such items as angle of attack, rate of rotation, etc., systematically. Rather, it is possible to change only the control settings of any given model loading and configuration. Consequently, several different loadings

and configurations were used, primarily to obtain a sufficient quantity of data and a sufficient range of important parameters.

A study of existing data (unpublished) of the spin characteristics of numerous models tested in the Langley free-spinning tunnels indicates that the range of spin conditions of the investigation presented herein is fairly wide and the results of the present investigation may therefore be taken as a general indication of the order of magnitude and direction of the aerodynamic forces and moments acting in normal fully developed spins of a straight-wing airplane with both vertical and horizontal tails.

The following is a list of the various data presented and the tables and figures in which the data is found. The aerodynamic force and moment coefficients as measured on the 1/10-scale model and the free-spinning characteristics of the 1/20-scale model are presented in Table III in terms of full-scale values. A comparison of the approximate spin radius used on the rotary balance and the radius calculated from the measured resultant aerodynamic force is presented in Table V. Also presented in Table V are the values of the angle between the measured resultant aerodynamic force and the Z body axis when the angle is projected alternately into a horizontal plane (Ψ), into the XZ body plane, and into the YZ body plane. The effect of setting the rudder from with to against the spin on the aerodynamic force and moment coefficients of the 1/10-scale model and the corresponding recovery characteristics of the 1/20-scale model by rapid full rudder reversal are presented in Table VI. The difference in

aerodynamic yawing-moment coefficients between the rudder-with and rudder-against settings is plotted against angle of attack of the model in Figure 17 and the total aerodynamic yawing-moment coefficient of the model with the rudder set against the spin is plotted in Figure 18. The results of tests performed on the 1/10-scale model with the horizontal tail in the original and rearward positions (Figure 12), with the spinning conditions held constant, are presented in Table VII and show the effect on the aerodynamic force and moment coefficients of unshielding the vertical tail by movement of the horizontal tail. The increments of yawing-moment coefficients caused by rudder reversal for the two horizontal-tail positions are presented in Table VIII and Figure 19. The effect of deflecting the landing flaps on the aerodynamic moment coefficients is shown in Table IX.

The inertia force and moment coefficients calculated for the fully developed spins are compared with the measured aerodynamic force and moment coefficients in Table X.

DISCUSSION OF RESULTS

General Aerodynamic Characteristics in Spins

The results of the force and moment measurements (Table III) show that, for the spins presented, the normal-force and longitudinal-force coefficients and the pitching-moment coefficients always had negative values. In other words, in an erect spin (positive angle of attack) the aerodynamic normal force always acted upward and toward the center of rotation, the aerodynamic longitudinal force always acted toward the

rear of the airplane, and the aerodynamic pitching moment was always a nose-down moment as would normally be expected for a conventional airplane at a positive angle of attack. The nose-down aerodynamic pitching-moment coefficient and the upward normal-force coefficient increased as the angle of attack increased.

The results of the rolling-moment measurements presented herein and other unpublished data indicate that the ailerons were approximately one-half or less as effective in producing rolling-moment coefficients above the stall as below the stall. The rolling-moment coefficient, however, varied in the same manner with aileron deflection above and below the stall; that is, when the ailerons were set to simulate a stick position to the right (rotation to the right), a positive rolling-moment coefficient was generally obtained, and when the ailerons were set to simulate a stick position to the left, a negative rolling-moment coefficient was obtained. No consistent variation in the lateral-force coefficient resulting from the variations in the spinning conditions tested was noted. The aerodynamic yawing-moment coefficients as measured were always antispin (negative for the right spins presented), even with the rudder set full with the spin. For these tests, therefore, the sign of the yawing-moment coefficient is the same as the sign of the sideslip angle at the tail, which was always outward or negative for the right spins tested.

Relation of the Aerodynamic Characteristics to the Inertia Characteristics in Spins

In a fully developed spin, the aerodynamic forces and moments acting on an airplane must be balanced by the inertia forces and moments produced by the rotating mass of the airplane in order to obtain a condition of dynamic equilibrium. Components of the resultant of the normal, longitudinal, and lateral aerodynamic forces balance the weight and the centrifugal force of the rotating airplane. Similarly, the aerodynamic pitching moment balances the inertia pitching moment of the rotating airplane, and the aerodynamic rolling and yawing moments balance inertia rolling and yawing moments, respectively. The equations of the inertia and aerodynamic moments as presented in Reference 17 from Euler's dynamical equations are as follows:

Rolling moment:

$$(I_Y - I_Z)qr - I_X \frac{dp}{dt} = -L \tag{2}$$

Pitching moment:

$$(I_Z - I_X)pr - I_Y \frac{dq}{dt} = -M \tag{3}$$

Yawing moment:

$$(I_X - I_Y)qp - I_Z \frac{dr}{dt} = -N \tag{4}$$

where

$$p = \Omega \cos \alpha \tag{5}$$

$$q = \Omega \sin \phi \tag{6}$$

$$r = \Omega \sqrt{\sin^2 \alpha - \sin^2 \phi} \tag{7}$$

These equations were developed for use about the principal axes of inertia but are used herein about the body axes. Possible discrepancies from using these equations about the body axes are considered to be negligible in that the angles between the body axes and principal axes are small. A general discussion of the equations of the spinning motion is made in Appendix B.

In these equations, the values on the right-hand side of the equations are the aerodynamic moments that result from the motion of the airplane in a spin. The sum of the values on the left-hand side of the equations is the sum of the inertia moments. The terms of the inertia equations dependent on the time rate of change of p, q, and r are the acceleration terms that would be zero in a completely steady spin. The values measured on the rotary balance are equal to the values on the right-hand side of the equations for steady spin conditions. As previously indicated, for the spins investigated, the free-spinning model oscillated slightly and the aerodynamic coefficients were measured for average values of the spin parameters determined in the free spins. The values of aerodynamic forces and moments as measured on the balance therefore appear to be approximate averages of the unsteady values existent in the actual spins.

Consideration of equations for equilibrium indicates certain conclusions regarding spinning equilibrium. For the pitching moment, the inertia effect depends on p, r, and $I_Z - I_X$. The inertia pitching moment will always be positive because the value of $I_Z - I_X$ is positive and p and r have the same sign and, therefore, their product

will always be positive. For the attainment of equilibrium, the aerodynamic pitching moments must be negative. The values of aerodynamic pitching moment measured (Table III) are all negative.

The sign of the inertia rolling moment depends on the signs of $I_Y - I_Z$ and of the product of r and q. For normal designs $I_Y - I_Z$ is always negative, and the product of r and q, which can change the sign of the inertia rolling moment, depends on whether the value of $\sin \phi$ is positive or negative. As was previously noted (Table III), the direction of the measured aerodynamic rolling moment changed and in general varied primarily with aileron position. The sign of ϕ has been observed for tests of numerous models (unpublished data) and, as is indicated in Table III, has been found to have a variation with aileron position similar to that for the measured aerodynamic rolling moment. In general, when the ailerons were with the spin (stick right in a right spin), the values of ϕ were positive (Table III); therefore, the inertia rolling moments were negative, and positive aerodynamic rolling moments were needed for equilibrium. When the ailerons were with the spin, the measured aerodynamic rolling moments were positive (Table III). Conversely, when the ailerons were against the spin, the values of ϕ generally were negative and thus the inertia rolling moments were positive and negative aerodynamic rolling moments were required for equilibrium. With the ailerons against the spin, the measured aerodynamic rolling moments were generally negative.

An examination of the equilibrium equation for yawing moment indicates that the inertia yawing moment is dependent on the sign of ϕ.

Because the sign of ϕ varied for the spins investigated (Table III), the inertia yawing moment would also change sign. All the values of the measured aerodynamic yawing moments (Table III), however, were negative (or antispin); consequently, when ϕ was positive, the aerodynamic and inertia yawing moments were of like sign and the requisites for spinning equilibrium were not fulfilled. The 1/20-scale model, however, actually spun for the cases presented herein and therefore had values of inertia moment coefficients equivalent to those calculated and presented in Table X within fairly close limits. At least some of the measured aerodynamic yawing moments therefore may be in error.

Generally the measured aerodynamic yawing-moment coefficients were too large against the spin; thus the sideslip angles set on the rotary balance may have been too large outward. The fact that the radii set on the balance were only approximate (previously discussed) could account for some change in angle of sideslip. The differences between the approximate radii set on the rotary balance and radii calculated from the measured aerodynamic force coefficients (Table V) indicate that the radii tested were generally larger than the actual radii of the spin. Examination of the equation for the sideslip at the center of gravity

$$\beta_{cg} = \phi - \tan^{-1} \frac{\Omega R_s \cos \Psi}{V} \qquad (8)$$

indicates that such a reduction in radius and any amount of the angle Ψ (angle between the projection of the resultant-force vector and the projection of the Z body axis in a horizontal plane) would reduce the outward sideslip (or increase the inward sideslip) of the actual spin

over that tested on the rotary balance. The differences in radii and the angle Ψ, therefore, do account for some changes in angle of sideslip and therefore could account in part for some of the discrepancy in the measured aerodynamic yawing-moment coefficients.

Another factor that may be considered is that the inertia moment coefficients presented herein are based on the steady-state portion of Euler's equations and do not include the effect of any oscillations which may have existed on the free-spinning model. An integration of the effects of oscillations for one or more complete turns, however, would probably be zero and, as previously indicated, the data presented would be the average for one or more complete turns of the spin. Further explanation of this lack of equilibrium between the aerodynamic and inertia yawing-moment coefficients is not readily available, and further study of this matter by iterative testing seems desirable.

As previously indicated, the measured aerodynamic yawing-moment coefficients were too large against the spin. Unpublished data of a contemporary investigation have indicated, however, that the instantaneous slopes of the variations of C_n with rudder deflection are approximately the same for each angle of attack above the stall, a result which is also generally true for the variation of C_n with sideslip angle and of C_n with spin coefficient. These results indicate that increments of measured aerodynamic yawing-moment coefficient ΔC_n presented herein may be considered accurate even though the total aerodynamic yawing-moment coefficients are generally conservatively large.

The comparison of the aerodynamic forces and moments (Table X) indicates slight differences in the rolling and pitching moments, as well as the differences in yawing moments previously discussed. The differences in the rolling and pitching moments were generally in magnitude and not in sign, as was the case for the yawing moments. The differences in the rolling moments were used to determine incremental values of the angle ϕ which, when used in Euler's dynamical equation, would account for the differences in the rolling moments. An average incremental value of ϕ of approximately 2.0° was obtained for all tests and is not believed to be unreasonable if the over-all limits of the test procedures are considered. A change in ϕ of this order of magnitude generally was not sufficient to influence the lack of equilibrium in the yawing-moment coefficients previously discussed.

The differences in the pitching moments were used to determine incremental values of the rate of rotation Ω which, when used in Euler's dynamical equations for pitching moment, would account for the differences in pitching moments. An average incremental value of Ω of approximately -0.12 radian per second (full-scale) was obtained for all tests and is considered to be relatively small with regard to spinning.

To summarize, it has been indicated that the rolling-moment and pitching-moment coefficients and the increments in yawing-moment coefficients presented herein are relatively accurate. The total aerodynamic yawing moments, however, are generally too large against the spin and, therefore, requirements based on the total aerodynamic yawing-moment coefficients are considered to be conservative.

Effect of Rudder Reversal on Aerodynamic Coefficients

The results of spin-tunnel tests of numerous models have indicated that the rudder can normally be an effective control for recovery from spins. This fact is true particularly when the mass of the airplane is distributed primarily along the fuselage (References 4 and 6). Many current airplanes of rocket- and jet-propelled designs have this type of loading and most of the free-spinning tests, presented herein for comparison with balance data, were made with such a weight distribution.

Accordingly, the aerodynamic force and moment coefficients in a spin were determined when the rudder was set with the spin and when the rudder was set against the spin. The results of these tests are given in Table VI in terms of the incremental differences in the moment and force coefficients with the rudder set with and against the spin. The primary effect of rudder reversal on the rigidly mounted 1/10-scale model was a relatively large increment of antispin yawing-moment coefficient when compared with the aerodynamic yawing-moment coefficient that existed for the fully developed spin. The other force and moment coefficients were affected to only a small degree, the increments resulting from the change in rudder setting being relatively small when compared with the aerodynamic coefficients which existed in the fully developed spin. Reversal of the rudder on the free-spinning model generally resulted in immediate changes in model attitude and rate of rotation which initially resulted from changes in the forces and moments similar to those measured on the 1/10-scale model.

The variation of the increment of yawing-moment coefficient with angle of attack is shown in Figure 17 and indicates that below an angle of attack of approximately 30° the value of the increment of the yawing-moment coefficient caused by rudder reversal is much larger than the value of the increment of yawing-moment coefficient obtained for spins above 30° angle of attack. The variation in rudder effectiveness with angle of attack appears to be primarily the result of the shielding the rudder by the horizontal tail. Smoke-flow tests on a spinning airplane (Reference 18) indicate the existence of such a shielding or blanketing effect of the horizontal tail on the vertical tail and rudder. A study of the tail-damping power factors and their components for the various tail configurations tested (Table IV) and of the increments of yawing-moment coefficients caused by setting the rudder against the spin (Table VI and Figure 17) indicates that at any given angle of attack the tail configuration that had the largest unshielded rudder volume coefficient consistently had the largest value of ΔC_n. The trends indicated by the tail-damping power factor (Reference 4) therefore seem to be in agreement with actual yawing-moment measurements in that the tail configurations having the largest calculated values of unshielded rudder volume coefficient had the largest values of ΔC_n caused by rudder reversal. The scatter of points or the variation of ΔC_n at any given angle of attack shown in Figure 17 is in part the result of these differences in rudder effectiveness. Also, at any given angle of attack, some scatter may result from a variation in sideslip for the various spin conditions tested for any given tail configuration.

Also indicated in Figure 17 and Table VI are those spins for which recoveries were satisfactory (2-1/4 turns or less) and those for which recoveries were not satisfactory by rudder reversal alone. The satisfactory recoveries generally were obtained by rudder reversal alone for spins in which ΔC_n was of the magnitude of 0.012 or greater, against the spin. Such values of ΔC_n were obtained only for spins in which the angle of attack was 30° or less. An exception was test 11 for which it was necessary to move the elevator, as well as the rudder, for satisfactory recovery. For test 11, the dynamic model was ballasted so that the weight was distributed primarily along the wings (loading 2, Table II) and References 4, 5, and 19 indicate that, for designs with the loading distributed primarily along the wings, the elevator became the predominant control for recovery. For such loadings, therefore, in spite of the ability of the rudder to produce a large increment of antispin yawing moment, movement of the elevator for recovery may be essential.

Total Aerodynamic Yawing Moment Required to Obtain Satisfactory Spin Recovery

A previous spin-balance investigation (Reference 7) has indicated that an aerodynamic yawing-moment coefficient of the order of 0.020 against the spin would be required to be supplied by parts of the airplane (including interference effects) other than the wing to prevent equilibrium in a steady spin or to obtain recovery from a steady spin. A later paper (Reference 9) indicates that a value of aerodynamic yawing-moment coefficient of 0.025 against the spin would

be necessary to prevent equilibrium in a steady spin. Subsequent free-spinning-tunnel experience has indicated that spin and recovery requirements should be based on the attainment of satisfactory spin recoveries (2-1/4 turns or less) and not just on recovery alone or the prevention of equilibrium in a spin because a design that has aerodynamic characteristics sufficient to prevent equilibrium in a steady spin may not be adequate for a satisfactory recovery. A requirement based on the amount of aerodynamic yawing-moment coefficient required to obtain satisfactory spin recovery therefore seems to be appropriate, and accordingly the following discussion is based on this premise. The results of force and moment measurements and of dynamic-model recovery tests were used to indicate the amount of total aerodynamic yawing-moment coefficient required for satisfactory recovery. Because of discrepancies previously discussed, these results may be considered conservative. The brief study presented was confined to measurements made with the rudder set against the spin, in that recoveries were obtained only for this rudder setting. The requirements discussed are applicable only to designs with geometric configurations similar to and with mass distributions and relative densities of the same order of magnitude as the present configurations.

The total aerodynamic yawing-moment coefficients of the model with the rudder set against the spin for the various tests performed are presented in Figure 18. Also shown in Figure 18 are those cases for which satisfactory recoveries were obtained and those for which unsatisfactory recoveries were obtained. As is indicated in Figure 17,

recoveries from the spins at angles of attack of 30° or less were generally satisfactory. The maximum total aerodynamic yawing-moment coefficient against the spin existent for these satisfactory recoveries was of the order of magnitude of 0.021. From a conservative viewpoint, it would appear that a value of total aerodynamic yawing-moment coefficient ranging from approximately 0.021 to 0.025 (antispin) would be adequate for satisfactory recovery from steep spins. This value compares with that indicated from previous spin-balance work in that it was estimated from References 9 and 11 that the wing of the present investigation contributes very little to the total aerodynamic yawing-moment coefficient. A value ranging from 0.021 to 0.025 for steep spins appears, therefore, to be in agreement with the value previously indicated as required to be supplied by parts of the airplane other than the wing. The wing, however, may contribute a prospin aerodynamic yawing moment, as is generally indicated for steep spins (References 7, 9, and 11). The requirement presented herein for satisfactory spin recovery from steep spins therefore may be more stringent than the requirement indicated in previous spin-balance investigations for the prevention of equilibrium in a steady spin.

In general, satisfactory recoveries were not obtained above 30° angle of attack (Figure 18) although some spins having angles of attack greater than 50° had total yawing-moment coefficients of the same order of magnitude as those for which satisfactory recoveries were attained below 30° angle of attack. Because satisfactory recoveries generally were not obtained for spins at angles of attack above 30°, the data

were not sufficient to determine the total amount of aerodynamic yawing-moment coefficient necessary for satisfactory recovery from any spin. It would appear, however, that the total aerodynamic yawing-moment coefficient against the spin required for satisfactory spin recovery may vary with angle of attack, increasing as the angle of attack increases, and that values larger than 0.025 may be required since values approaching 0.020 were obtained at high angles of attack for some of the cases presented herein and the recoveries were unsatisfactory. This fact further indicates that the previous requirement (References 7 and 9) is not applicable for satisfactory recoveries from spins.

Previous discussion of the increments of yawing-moment coefficients resulting from rudder reversal has indicated that for airplane loadings for which rudder movement is required for satisfactory recovery, an increment of aerodynamic yawing-moment coefficient of the order of 0.012 or greater may lead to satisfactory recovery for steep spins and the discussion indicates that a total aerodynamic yawing-moment coefficient of the order of 0.025, which was previously mentioned as being a conservative value, may lead to satisfactory recoveries for the same conditions. For flatter spins, however, and for loading conditions for which the rudder is the primary control for recovery (Reference 4) it is not known whether a requirement for satisfactory recovery should be based on the increment of aerodynamic yawing-moment coefficient caused by rudder reversal or on the total aerodynamic yawing-moment coefficient. It appears, however, that in either case the amount of

incremental or total aerodynamic yawing-moment coefficient required may increase with angle of attack; whereas the amount of yawing-moment coefficient available may generally decrease with angle of attack. Thus, the danger of a flat spin and the necessity for properly designing airplanes to obtain relatively steep spins are indicated.

Effect of Horizontal-Tail Position on Aerodynamic Coefficients and Rudder-Reversal Effectiveness

Only one of the several tail modifications tested was effective in improving the spin-recovery characteristics of the original configuration. For the present study, the results for the other modifications were used only as means of extending the range of spinning attitudes for which data were made available. The effective modification (modification 1) was the one in which the horizontal tail was moved 15 inches (full-scale) rearward of the original position (Figure 12).

A study of the results of tests, in which force and moment measurements were made with the horizontal tail in both the original and revised positions for spinning attitudes obtained on the dynamic model with the original tail position (Tables VII and VIII), indicates changes in the forces and moments to which the improvement in the spin and recovery characteristics obtained by the rearward horizontal-tail movement may be attributed. When the rudder was with the spin (Table VII), moving the horizontal tail rearward led to an increase in the nose-down pitching-moment coefficient and to a slight decrease in the antispin yawing-moment coefficient. The effect of these aerodynamic changes for the free-spinning tests was generally to decrease the angle of attack

of the spin for any given control configuration. The effect on the yawing-moment coefficient (Table VII) is in general accord with the indications of tail-damping power factor (Reference 4), a factor which is based on the tail geometric measurements and is used as an indication of the tail power in effecting spin recovery. Calculations of tail-damping power factor for modification 1 (Table IV) show a decrease in tail-damping ratio and an increase in unshielded rudder volume coefficient which would lead to a decrease in the antispin yawing-moment coefficient when the rudder was with the spin.

A comparison of the increments of yawing-moment coefficients resulting from rudder reversal for the model with the horizontal tail in the original position and with the horizontal tail moved rearward is presented in Table VIII. When the horizontal tail was in the original position, the increments of yawing-moment coefficient were relatively small and in some cases were positive; this result may be attributed to some interference effects on the shielded rudder. When the horizontal tail was in the rearward position, the increments of yawing-moment coefficient were generally relatively large and negative (antispin). Inasmuch as only the horizontal tail was moved, the increase in the increment of antispin yawing moment due to reversing the rudder (or rudder-reversal effectiveness) was caused by the unshielding of the rudder. In order to illustrate further the increase in rudder-reversal effectiveness due to the unshielding of the rudder, a plot of incremental yawing-moment coefficient due to rudder reversal with the horizontal

tail in the original position against the incremental yawing-moment coefficient obtained with the horizontal tail in the rearward position (Figure 19) shows that in all cases the greatest rudder-reversal effectiveness was obtained with the revised tail.

This investigation shows primarily the effect of unshielding the rudder in spinning attitudes. Movement of the horizontal tail rearward as was done in the present investigation may not necessarily unshield the rudder for other airplane tail designs.

Effects of Lowering Landing Gear and Deflecting Flaps on Spin Attitudes and Aerodynamic Coefficients

The effects of lowering the landing gear and deflecting the flaps on the spin attitudes and aerodynamic force and moment coefficients are shown in Table III. Only slight differences were obtained between the spin attitudes with the flaps deflected and landing gear down, and with only the flaps deflected. These results are in agreement with a complete study of the effects of landing gear and flaps on spin recovery characteristics (Reference 20) in that the landing gear has only a slight effect. The force measurements in Table III also show little effect of the landing gear. The results of the free-spinning tests presented in Table III, however, indicated an adverse effect of deflecting the flaps in that the spins were somewhat flatter when the flaps were deflected.

In order to study the effects of flaps on the rudder-reversal effectiveness, several tests were made on the balance with the model

set at arbitrary attitudes and control settings. For each attitude and control setting, the flaps were deflected and retracted, and the results are presented in Table IX. The increments of yawing-moment coefficient resulting from setting the rudder from with to against the spinning rotation were much larger when the flaps were up than when they were deflected; thus a definite adverse effect of flaps on the rudder was indicated. These results are in good agreement with the results of Reference 20 which indicate an adverse effect of deflecting the flaps on recovery characteristics.

CONCLUSIONS

The following conclusions regarding aerodynamic characteristics in spins are based on the aerodynamic forces and moment coefficients measured on a 1/10-scale model of a fighter airplane in spinning conditions simulating those obtained previously for a similar dynamic model and in other arbitrary spinning conditions:

1. The primary effect of rudder reversal was to give a relatively large increment of antispin yawing-moment coefficient when compared with the aerodynamic yawing-moment coefficient of the fully developed spin. The other force and moment coefficients were affected to a much less degree.

2. The increment of yawing-moment coefficient obtained by rudder reversal in spins was much larger at low angles of attack than at high angles of attack; this result indicates that more rudder-reversal effectiveness was obtained in steep spins because of less rudder shielding.

3. Unshielding the rudder by movement of the horizontal tail rearward increased the rudder-reversal effectiveness.

4. Downward deflection of landing flaps reduced the rudder-reversal effectiveness.

5. A total aerodynamic yawing-moment coefficient ranging from approximately 0.021 to 0.025, antispin, may be required for satisfactory recoveries from steep spins based on a conservative estimate from the experimental results. Larger values of yawing-moment coefficient may be necessary for satisfactory recovery from flatter spins.

Consideration of the results obtained indicate that certain valuable information has and may be obtained from the rotary balance. One disturbing factor exists, however, which indicates that further studies and improvements of the techniques and equipment are necessary. This fact is that the exact conditions of fully developed spinning equilibrium were not duplicated on the balance, as indicated by the difference in aerodynamic and inertia force and moment data listed on Table X. It appears that methods of more accurately determining the radius of spin of a free-spinning model is important. Generally it would appear that more accurate measurements of free spin are necessary either by the use of two or more motion-picture cameras, rather than the one now used, to record the model motion, or by installing accelerameters in the model which would allow an accurate evaluation of the centrifugal force in the spin and therefore the radius of the spin. It appears that methods of setting the angle Ψ (discussed previously) on the rotary balance to more accurately reproduce the actual spinning

attitude is a necessity. With these suggestions and by methods of iterative or systematic testing, it seems logical that spinning equilibriums may accurately be reproduced, and thus for further work spinning equilibrium may be accurately determined by rotary balance tests.

After accomplishing the above-mentioned conditions, a general study for spinning motions and conditions of equilibrium may be made. The results of numerous different configurations could be obtained and their conditions of spin equilibrium and how the equilibrium is influenced by changes in weight, moments of inertia, etc., may be determined. The effects of control settings and movements on the aerodynamic forces and moments may be measured and their influence on the motion of the spin may be determined.

The rotary balance may be used to determine some of the stability derivatives (those associated with rolling velocity P) which is one of some consequence in normal stability work. Further, these derivatives can be determined at and near the stalling angle of attack (angle of attack of maximum lift) and the influence of these derivatives at and subsequent to the stall may be determined.

REFERENCES

1. Gates, S. B., and Bryant, L. W.: The Spinning of Aeroplanes. ARC RM No. 1001.

2. Crowe, J. H.: An Elementary Study of the Spin. Aircraft Engineering, Feb. 1939 pp. 39-43, 54, March 1939 pp. 111-114, April 1939 pp. 158-160, May 1939 pp. 203-208, July 1939 pp. 273-278.

3. Zimmerman, C. H.: Preliminary Tests in the N.A.C.A. Free-Spinning Wind Tunnel. NACA Rep. 557, 1936.

4. Neihouse, Anshal I., Lichtenstein, Jacob H., and Pepoon, Philip W.: Tail-Design Requirements for Satisfactory Spin Recovery. NACA TN 1045, 1946.

5. Neihouse, A. I.: Tail-Design Requirements for Satisfactory Spin Recovery for Personal-Owner-Type Light Airplanes. NACA TN 1329, 1947.

6. Stone, Ralph W., Jr., and Klinar, Walter J.: The Influence of Very Heavy Fuselage Mass Loadings and Long Nose Lengths upon Oscillations in the Spin. NACA TN 1510, 1948.

7. Bamber, M. J., and Zimmerman, C. H.: Spinning Characteristics of Wings. I - Rectangular Clark Y Monoplane Wing. NACA Rep. 519, 1935.

8. Bamber, M. J.: Spinning Characteristics of Wings. II - Rectangular Clark Y Biplane Cellule: 25 Percent Stagger; 0° Decalage; Gap/Chord 1.0. NACA TN 526, 1935.

9. Bamber, M. J., and House, R. O.: Spinning Characteristics of Wings. III - A Rectangular and a Tapered Clark Y Monoplane Wing with Rounded Tips. NACA TN 612, 1937.

10. Bamber, M. J., and House, R. O.: Spinning Characteristics of Wings. IV - Changes in Stagger of Rectangular Clark Y Biplane Cellules. NACA TN 625, 1937.

11. Bamber, M. J., and House, R. O.: Spinning Characteristics of Wings. V - N.A.C.A. 0009, 23018, and 6718 Monoplane Wings. NACA TN 633, 1938.

12. Bamber, M. J., and Zimmerman, C. H.: Effect of Stabilizer Location upon Pitching and Yawing Moments in Spins as Shown by Tests with the Spinning Balance. NACA TN 474, 1933.

13. Bamber, M. J., and Zimmerman, C. H.: The Aerodynamic Forces and Moments Exerted on a Spinning Model of the "NY-1" Airplane as Measured by the Spinning Balance. NACA Rep. 456, 1933.

14. Bamber, M. J., and Zimmerman, C. H.: The Aerodynamic Forces and Moments on a Spinning Model of the F4B-2 Airplane as Measured by the Spinning Balance. NACA TN 517, 1935.

15. Bamber, M. J., and House, R. O.: Spinning Characteristics of the XN2Y-1 Airplane Obtained from the Spinning Balance and Compared with Results from the Spinning Tunnel and from Flight Tests. NACA Rep. 607, 1937.

16. Jacobs, E. N., and Sherman, A.: Airfoil Section Characteristics as Affected by Variations of the Reynolds Number. NACA TR 586.

17. Webster, Arthur Gordon: The Dynamics of Particles and of Rigid, Elastic, and Fluid Bodies. Third ed., G. E. Stechert and Co., New York, 1942, pp. 260-261.

18. Scudder, N. F., and Miller, M. P.: The Nature of Air Flow about the Tail of an Airplane in a Spin. NACA TN 421, 1932.

19. Neihouse, A. I.: A Mass-Distribution Criterion for Predicting the Effect of Control Manipulation on the Recovery from a Spin. NACA ARR, Aug. 1942.

20. Gale, Lawrence J.: Effect of Landing Flaps and Landing Gear on the Spin and Recovery Characteristics of Airplanes. NACA TN 1643, 1948.

21. Berman, Theodore: Comparison of Model and Full-Scale Spin Test Results for 60 Designs. NACA TN 2134, July 1950.

22. Malvestuto, Frank S., Jr., and Gale, Lawrence J.: Formulas for Additional Mass Corrections to the Moments of Inertia of Airplanes. NACA MR, April 3, 1946.

23. Neihouse, Anshal I., and Pepoon, Philip W.: Dynamic Similitude between a Model and a Full-Scale Body for Model Investigation at Full-Scale Mach Number. NACA TN 2062, March 1950.

APPENDIX A

SCALE RELATIONS AND RULES OF SIMILARITY BETWEEN MODEL AND AIRPLANE FREE-SPINNING RESULTS

In order to evaluate the results of free-spinning tunnel tests so as to determine how full-scale airplanes will spin and recover from spins, it is necessary to establish certain relations between model motions and airplane motions. First, of course, it is necessary that the model and the full-scale airplane be geometrically similar. That is all dimensions of the model are $\frac{1}{n}$ times the dimensions of the airplane. The following table lists these geometric relations

$$l_m = \frac{1}{n} l_{fs} \tag{A1}$$

$$A_m = \frac{1}{n^2} A_{fs} \tag{A2}$$

$$v_m = \frac{1}{n^3} v_{fs} \tag{A3}$$

where l, A, and v are length, area, and volume, and where the subscripts m and fs are model and full-scale respectively, and n is the scale factor.

Next it is necessary to consider the forces and moments acting on the model and airplane. The weight and centrifugal force are the mass forces acting on a spinning model or airplane,

$$M_m g = C_{1m} \frac{1}{2} \rho_{am} V_m^2 S_m$$

$$M_{fs} g = C_{1fs} \frac{1}{2} \rho_{afs} V_{fs}^2 S_{fs}$$

and

$$\frac{M_m \rho_{afs}}{M_{fs} \rho_{am}} = \frac{C_{1m}}{C_{1fs}} \frac{V_m^2}{V_{fs}^2} \frac{1}{n^2} \qquad (A4)$$

also

$$M_m l_m \Omega_m^2 = C_{2m} \frac{1}{2} \rho_{am} V_m^2 S_m$$

$$M_{fs} l_{fs} \Omega_{fs}^2 = C_{2fs} \frac{1}{2} \rho_{afs} V_{fs}^2 S_{fs}$$

and

$$\frac{M_m \rho_{afs}}{M_{fs} \rho_{am}} = \frac{C_{2m}}{C_{2fs}} \frac{V_m^2}{V_{fs}^2} \frac{\Omega_{fs}^2}{\Omega_m^2} \frac{1}{n} \qquad (A5)$$

where ρ_a is air density, V is velocity, C_1 and C_2 are aerodynamic coefficients, and Ω is the rate of rotation of the spin.

Equating Equations (A4) and (A5) and presuming that the aerodynamic coefficients

$$C_{1m} = C_{1fs} \quad \text{and} \quad C_{2m} = C_{2fs}$$

the following result is obtained

$$\frac{1}{n^2} = \frac{fs^2}{m^2}\frac{1}{n}$$

$$\Omega_m = \Omega_{fs}\sqrt{n} \tag{A6}$$

All moments in a spin are similar in form and may be expressed characteristically as

$$I_m\Omega_m^2 = C_{3m}\frac{1}{2}\rho_{am}V_m^2 S_m l_m$$

$$I_{fs}\Omega_{fs}^2 = C_{3fs}\frac{1}{2}\rho_{afs}V_{fs}^2 S_{fs} l_{fs}$$

and

$$\frac{I_m\rho_{afs}n}{I_{fs}\rho_{am}} = \frac{C_{3m}}{C_{3fs}}\frac{V_m^2}{V_{fs}^2}\frac{1}{n^3} \tag{A7}$$

Now $I = ml^2$ and further presuming that $C_{3m} = C_{3fs}$ the following is obtained

$$\frac{M_m l_m^2}{M_{fs} l_{fs}^2}\frac{\rho_{afs}}{\rho_{am}} = \frac{V_m^2}{V_{fs}^2}\frac{1}{n^4}$$

$$\frac{M_m\rho_{afs}}{M_{fs}\rho_{am}} = \frac{V_m^2}{V_{fs}^2}\frac{1}{n^2} \tag{A8}$$

which is identical to Equation (A4).

Consider now the mass and air density. By necessity, the model results in the 20-foot spin tunnel are obtained at sea level density whereas the corresponding airplane operates at some relatively high altitude. In order to eliminate the effect of the differences in air density, it is necessary to make the relative density between the model and air and the airplane and air the same, thus

$$M_m \rho_{afs} = l_m^3 \rho_m \rho_{afs}$$

$$M_{fs} \rho_{am} = l_{fs}^3 \rho_{fs} \rho_{afs}$$

and if $\rho_m \rho_{afs}$ is made equal to $\rho_{fs} \rho_{am}$ then

$$\frac{M_m \rho_{afs}}{M_{fs} \rho_{am}} = \frac{l_m^3}{l_{fs}^3} = \frac{1}{n^3}$$

Equation (A4) or (A8) thus may be rewritten as

$$\frac{V_n^2}{V_{fs}^2} \frac{1}{n^2} = \frac{1}{n^3}$$

and

$$V_m = V_{fs} \sqrt{\frac{1}{n}} \qquad (A9)$$

If further consideration is given of the time of motions the following may be written

$$V_m = \frac{dl_m}{dt_m} = V_{fs}\sqrt{\frac{1}{n}} = \frac{dl_{fs}}{dt_{fs}}\sqrt{\frac{1}{n}}$$

$$\frac{t_m}{t_{fs}} = \frac{l_m}{l_{fs}}\sqrt{n} = \sqrt{\frac{1}{n}}$$

and

$$t_m = \frac{1}{n}\, t_{fs} \tag{A10}$$

This implies that the model travels a model length in $\frac{1}{n}$ times the time required by the airplane to travel a corresponding full scale length. Further consider the angular velocities

$$\Omega_m = \frac{da_m}{dt_m} = \Omega_{fs}\sqrt{n} = \frac{da_{fs}}{dt_{fs}}\sqrt{n}$$

$$\frac{a_m}{a_{fs}} = \frac{t_m}{t_{fs}}\sqrt{n}$$

and

$$a_m = a_{fs} \tag{A11}$$

(where a is angular displacement) by substitution from Equation (A10). This implies that the model and airplane turn through the same angle while traveling corresponding lengths.

The spin coefficient $\frac{\Omega b}{2V}$ used in this paper is a nondimensional parameter and therefore

$$\frac{\Omega_m l_m}{2V_m} = \frac{\Omega_{fs}\sqrt{n}\ l_{fs}\sqrt{n}}{n2V_{fs}} = \frac{\Omega_{fs} l_{fs}}{2V_{fs}}$$

This shows that all helix angles described by the model are identical to those described by the airplane.

Froude number $\frac{V}{\sqrt{lg}}$ (the relationship between gravitational and inertia forces) was considered in the analysis presented herein when the scale relations of Equations (A4) and (A5) were considered simultaneously. Further evidence of this may be shown as

$$\frac{V_m}{\sqrt{l_m g}} = \frac{V_{fs}\sqrt{n}}{\sqrt{n}\sqrt{l_{fs} g}} = \frac{V_{fs}}{\sqrt{l_{fs} g}}$$

and assuming that the acceleration of gravity is the same for model and airplane, the Froude numbers are equal.

In the analysis presented, it has been assumed that the Reynolds number, $\frac{lV}{\nu}$ (the relation between viscous and inertia forces) has had no influence on the aerodynamic force and moment coefficients. This was done when the aerodynamic force and moment coefficients for the model and airplane were considered to be equal. If model and airplane Reynolds numbers were the same for the conditions noted herein it would be necessary that

$$\frac{l_m V_m}{\nu_m} = \frac{l_{fs} V_{fs}}{\nu_{fs}} = \frac{l_m n V_m \sqrt{n}}{\nu_{fs}}$$

and

$$\nu_m = \frac{\nu_{fs}}{(n)^{3/2}} \tag{A12}$$

The attainment of this equality appears generally impossible unless the model was to be tested in some medium other than air, having essentially greatly different viscous characteristics. Correlation of model and airplane results (Reference 21) has indicated generally, however, that different Reynolds numbers have not greatly influenced the results of free-spinning model tests, in that model and airplane results have been shown to be quite similar. This evidence primarily indicates that in spinning attitudes, aerodynamic force and moment coefficients are not fundamentally functions of Reynolds number. Lack of correlation for a recent high speed configuration, however, has indicated that in the future further study of the Reynolds effects in spins must be made.

The relationship indicated by Equation (A9) indicates indirectly that in the relationships established by this analysis, the Mach number has not been a consideration. For present configurations and operational altitudes this neglect has not been serious as the spinning rates of descent have been well below the speed of sound. However, larger wing loadings, cleaner designs, and higher operational altitudes may cause compressibility effects to become important in spins. Some considerations of Mach number on dynamic model motions have been made in Reference 23.

Thus, for the present, the Froude number is the primary similarity rule used in free-spinning tunnel work and in summary, the following basic relationships are used,

$$l_m = \frac{1}{n} l_{fs}$$

$$M_m = \frac{1}{n^3} M_{fs} \frac{\rho_{am}}{\rho_{afs}}$$

$$I_m = \frac{1}{n^5} I_{fs} \frac{\rho_{am}}{\rho_{afs}}$$

$$\Omega_m = \sqrt{n}\, \Omega_{fs}$$

$$V_m = \sqrt{\frac{1}{n}}\, V_{fs}$$

and

$$a_m = a_{fs}$$

APPENDIX B

The equations of motion which are normally associated to the spin are Euler's dynamical equations of motion. These equations are generally presented in most text books on Rigid Dynamics, as for example, Reference 17. In brief, these equations are derived as follows.

Consider a particle of mass in a rigid body which is rotating about each axis of a system of mutually perpendicular axes. The velocity components of this particle of mass are

$$\left.\begin{aligned} V_X &= (qZ - rY) \\ V_Y &= (rX - pZ) \\ V_Z &= (pY - qX) \end{aligned}\right\} \qquad (B1)$$

and

The accelerations of the particle are

$$\left.\begin{aligned} a_X &= \frac{dV_X}{dt} = Z\frac{dq}{dt} + q\frac{dZ}{dt} - y\frac{dr}{dt} - r\frac{dY}{dt} \\ a_Y &= \frac{dV_Y}{dt} = X\frac{dr}{dt} + r\frac{dX}{dt} - Z\frac{dp}{dt} - p\frac{dZ}{dt} \\ a_Z &= \frac{dV_Z}{dt} = Y\frac{dp}{dt} + p\frac{dY}{dt} - X\frac{dq}{dt} - q\frac{dX}{dt} \end{aligned}\right\} \qquad (B2)$$

and

The forces acting on this particle are therefore

$$\left.\begin{aligned} F_X &= -Ma_X \\ F_Y &= -Ma_Y \\ F_Z &= -Ma_Z \end{aligned}\right\} \qquad (B3)$$

and

The moments created by these forces about the various axis are

$$\left.\begin{aligned} L &= F_Z Y - F_Y Z \\ M &= F_X Z - F_Z X \\ N &= F_Y X - F_X Y \end{aligned}\right\} \qquad (B4)$$

and

Now by substitution from Equations (B1), (B2), and (B3)

$$\left.\begin{aligned} L &= -M\left[\left(Y^2 + Z^2\right)\frac{dp}{dt} + \left(Y^2 - Z^2\right)qr + YX\left(pr - \frac{dq}{dt}\right) - \right. \\ &\qquad \left. ZX\left(pq + \frac{dr}{dt}\right) + YZ\left(r^2 + q^2\right)\right] \\ M &= -M\left[\left(Z^2 + X^2\right)\frac{dq}{dt} + \left(Z^2 - X^2\right)pr - YX\left(qr + \frac{dp}{dt}\right) + \right. \\ &\qquad \left. ZY\left(qp - \frac{dr}{dt}\right) + XZ\left(p^2 - r^2\right)\right] \\ N &= -M\left[\left(X^2 + Y^2\right)\frac{dr}{dt} + \left(X^2 - Y^2\right)pq - YZ\left(rp + \frac{dq}{dt}\right) + \right. \\ &\qquad \left. ZX\left(rq - \frac{dp}{dt}\right) + XY\left(q^2 - p^2\right)\right] \end{aligned}\right\} \qquad (B5)$$

These moments are for one particle of mass and a summation of these moments for all particles in the body lead to the total moments acting on the body.

$$\Sigma\, M\left(Y^2 + Z^2\right) = I_X$$

$$\Sigma\, M\left(Z^2 + X^2\right) = I_Y$$

$$\Sigma\, M\left(X^2 + Y^2\right) = I_Z$$

$$\Sigma\, M\left(Y^2 - Z^2\right) = I_Z - I_Y$$

$$\Sigma\, M\left(Z^2 - X^2\right) = I_X - I_Z$$

$$\Sigma\, M\left(X^2 - Y^2\right) = I_Y - I_X$$

$$\Sigma\, M(XY) = I_{XY}$$

$$\Sigma\, M(XZ) = I_{XZ}$$

and

$$\Sigma\, M(YZ) = I_{YZ}$$

Further if the axis considered are the principal axes then the product of inertia terms I_{XY}, I_{XZ}, and I_{YZ} are zero and the total moments are

$$\left.\begin{aligned} L &= -I_X \frac{dp}{dt} + \left(I_Y - I_Z\right)qr \\ M &= -I_Y \frac{dq}{dt} + \left(I_Z - I_X\right)pr \end{aligned}\right\} \qquad (B6)$$

and

$$\left. N = -I_Z \frac{dr}{dt} + \left(I_X - I_Y\right)pq \right\}$$

Euler's dynamical equations.

For the spinning conditions considered in this paper the axis considered are the body axis. For airplanes, however, the principle axis and body axis are nearly coincident and Euler's equations were used. The products of inertia of the models used herein were not measured. For airplanes of course only the product of inertia I_{XZ} exists, because of symmetry about the X axis.

Inertia moments about other axis than principal axis such as the earth or wind axis as shown in Figure 20 are somewhat more complicated because of the products of inertia. About other axis than the principle axis the moments are

$$\left.\begin{aligned} L &= -I_X \frac{dp}{dt} + \left(I_Y - I_Z\right)qr + I_{XZ}\left(pq + \frac{dr}{dt}\right) \\ M &= -I_Y \frac{dq}{dt} + \left(I_Z - I_X\right)pr - I_{XZ}\left(p^2 - r^2\right) \\ N &= -I_Z \frac{dr}{dt} + \left(I_X - I_Y\right)pq - I_{XZ}\left(rq - \frac{dp}{dt}\right) \end{aligned}\right\} \qquad (B7)$$

and

These are the moments normally used for stability consideration about stability axis.

For steady state conditions as would exist in a steady fully developed spin, Equations (B6) and (B7) would be modified somewhat as the rates of change of p, q, and r with time would be zero.

The forces associated with the rotation along each of the various axis may be obtained by a summation of the particle forces given in

Equations (B3). If the origin of the axis was at the center of gravity, a summation of Equations (B3) would give zero and the resultant force due to rotation acting on the body would be (for steady conditions)

$$F = MR_g\Omega^2 \tag{B8}$$

This force may be broken down to its various components.

If the origin of the axis is considered to be at the center of rotation, however, a summation of Equations (B3) should lead to the components of the resultant force due to rotation

$$\left.\begin{aligned} F_X &= -M\left(Z\frac{dq}{dt} + q\frac{dZ}{dt} - Y\frac{dr}{dt} - r\frac{dY}{dt}\right) \\ F_Y &= -M\left(X\frac{dr}{dt} + r\frac{dX}{dt} - Z\frac{dp}{dt} - p\frac{dZ}{dt}\right) \\ \text{and} \\ F_Z &= -M\left(Y\frac{dp}{dt} + p\frac{dY}{dt} - X\frac{dq}{dt} - q\frac{dX}{dt}\right) \end{aligned}\right\} \tag{B9}$$

Now

$$\frac{dX}{dt} = V_X$$

$$\frac{dY}{dt} = V_Y$$

and

$$\frac{dZ}{dt} = V_Z$$

Therefore by substituting appropriate values from Equations (B1) in Equation (B8) the following is obtained

$$F_X = -M\left[Z\frac{dq}{dt} - Y\frac{dr}{dt} + q(pY - qX) - r(rX - pZ)\right]$$

$$F_Y = -M\left[X\frac{dr}{dt} - Z\frac{dp}{dt} + r(qZ - rY) - p(pY - qX)\right] \qquad (B10)$$

and

$$F_Z = -M\left[Y\frac{dp}{dt} - X\frac{dq}{dt} + p(rX - pZ) - q(qZ - rY)\right]$$

For steady state conditions, the rates of change of p, q, and r with time are zero and

$$\left.\begin{aligned} F_X &= -M\left[p(Yq + Zr) - X(q^2 + r^2)\right] \\ F_Y &= -M\left[q(Zr + Xp) - Y(r^2 + p^2)\right] \\ F_Z &= -M\left[r(Xp + Yq) - Z(p^2 + q^2)\right] \end{aligned}\right\} \qquad (B11)$$

and

The resultant force, $F = mR_s\Omega^2$ should also equal of course $\sqrt{F_X^2 + F_Y^2 + F_Z^2}$ as

$$\sqrt{F_X^2 + F_Y^2 + F_Z^2} = M\sqrt{p^2 + q^2 + r^2 \quad V_X^2 + V_Y^2 + V_Z^2}$$

$$R_s^2 = X^2 + Y^2 + Z^2$$

$$\Omega^2 = p^2 + q^2 + r^2$$

and

$$V = \sqrt{V_X^2 + V_Y^2 + V_Z^2} = R_s\Omega$$

therefore

$$\sqrt{F_X^2 + F_Y^2 + F_Z^2} = MR_s\Omega^2$$

In addition to this rotational force, there is of course a weight force, the total resultant force becomes

$$F_R = M\sqrt{R_s^2\Omega^4 + g^2} \tag{B12}$$

The components of the weight force are

$$F_{WX} = Mg \cos \alpha$$

$$F_{WY} = Mg \sin \phi \tag{B13}$$

and

$$F_{WZ} = Mg\sqrt{\sin^2\alpha - \sin^2\phi}$$

The addition of Equations (B10) and Equations (B13) give the total forces acting along each of the axes. The addition of Equations (B11) and (B13) give the forces acting in the steady state case.

The analysis presented here deals primarily with the mass moments and forces acting on a rotating rigid body. The aerodynamic moments and forces are of course at any given instant equal in magnitude and opposite in sign to these mass forces and moments.

TABLE I.- CORRESPONDING FULL-SCALE DIMENSIONAL

CHARACTERISTICS OF A FIGHTER MODEL

Wing span, ft	50.35
Length, over-all, ft	44.70
Wing:	
Area, sq ft	425.0
Section, root	NACA 65_{112}-213
Section, tip	NACA 65_{112}-213
Root-chord incidence, deg	2.5
Tip-chord incidence, deg	2.5
Aspect ratio	6.0
Sweepback of leading edge of wing, deg	0
Dihedral, leading-edge chord line, deg	6.0
Mean aerodynamic chord, in.	115.00
Leading edge of mean aerodynamic chord rearward of leading edge of wing, in.	0
Flaps:	
Chord, percent of wing chord	18.75
Area (rearward of hinge line), percent of wing area	12.55
Span, percent of wing span	44.0
Ailerons:	
Chord, percent of wing chord	20.00
Area (rearward of hinge line), percent of wing area	5.90
Span, percent of wing span	44.8
Horizontal tail surfaces:	
Total area, sq ft	108.0
Span, ft	23.33
Elevator area (rearward of hinge line), sq ft	30.0
Distance from normal center of gravity to elevator hinge line (original location of horizontal tail), ft	22.95
Vertical tail surfaces:	
Total area, sq ft	36.0
Rudder area (rearward of hinge line), sq ft	13.2
Distance from normal center of gravity to top of rudder hinge line, ft	23.05

TABLE II.- CORRESPONDING FULL-SCALE MASS CHARACTERISTICS OF A FIGHTER MODEL

[Moments of inertia are given about center of gravity]

	Loading	Weight (lb)	Center-of-gravity location		Relative airplane density, μ		Moments of inertia (slug-ft^2)			Mass parameters		
			$x/\bar{c}$	$z/\bar{c}$	Sea level	15,000 feet	I_X	I_Y	I_Z	$\frac{I_X - I_Y}{mb^2}$	$\frac{I_Y - I_Z}{mb^2}$	$\frac{I_Z - I_X}{mb^2}$
1	Normal	17,835	0.212	0.009	13.61	17.35	17,342	37,920	53,396	-147×10^{-4}	-110×10^{-4}	257×10^{-4}
2	Full alternate loading	22,200	.200	.052	13.50	21.41	39,900	37,880	75,700	11	-215	204
3	Partial alternate loading	20,350	.200	.052	12.42	19.68	29,600	37,250	65,900	-47	-178	225
4	Center of gravity, 7 percent $\bar{c}$ rearward of normal	17,940	.282	.009	10.95	17.40	16,190	34,621	50,977	-130	-115	245

TABLE III.- FREE-SPINNING CHARACTERISTICS OF $\frac{1}{20}$-SCALE MODEL AND AERODYNAMIC FORCE AND MOMENT COEFFICIENTS OF $\frac{1}{10}$-SCALE MODEL OF A FIGHTER AIRPLANE IN SPINS

[Data have been converted to full-scale values; rudder full with; right erect spins]

Test	Modification		Figure (a)	Model condition	Loading condition (table II)	Control deflections		Free-spinning characteristics							Aerodynamic force and moment coefficients					
						Elevator	Ailerons	α (deg)	ϕ (deg)	β_{cg} (deg)	β_t (deg)	Ω (rps)	V (fps)	$\frac{\Omega b}{2V}$	R_s (ft)	C_X	C_Y	C_Z	C_l	C_m	C_n
1	-------	None	---------	Clean	1	Full up	Full against	46	-1.4	-5.2	-12.0	0.304	243	0.199	8.53	-0.0682	-0.0365	-1.2464	-0.0106	-0.0841	-0.0025
2	-------do----------		---------	--------do---------	1	Neutral	-----do-----	63	.6	-1.4	-14.5	.394	197	.316	2.69	-.0254	-.0636	-1.5715	-.0011	-.1697	-.0087
3	-------do----------		---------	--------do---------	1	---do----	-----do-----	43	-3.6	-6.5	-17.3	.331	223	.234	8.08	-.0448	-.0278	-1.3282	-.0106	-.1107	-.0051
4	-------do----------		---------	--------do---------	1	Full down	-----do-----	42	-3.3	-6.1	-17.1	.414	210	.311	5.27	-.0698	-.0027	-1.4245	-.0050	-.1360	-.0033
5	-------do----------		---------	--------do---------	1	Full up	Neutral	50	2.0	-.2	-14.4	.503	223	.356	2.71	-.0520	-.0543	-1.4459	-.0013	-.1076	-.0068
6	-------do----------		---------	--------do---------	1	Neutral	-----do-----	35	.5	-4.4	-11.0	.358	243	.235	9.18	-.0734	.0005	-1.1715	.0075	-.0895	-.0016
7	-------do----------		---------	--------do---------	1	Full down	-----do-----	60	1.4	-1.0	-15.4	.372	190	.309	3.44	-.0201	-.0580	-1.6524	.0091	-.1750	-.0053
8	1	Horizontal tail moved rearward	9	--------do---------	1	Full up	Full against	46	.4	-3.4	-13.3	.345	216	.252	6.62	-.1040	-.0303	-1.3346	-.0072	-.0881	-.0033
9	1	----------do----------	9	--------do---------	1	Neutral	-----do-----	38	-1.4	-4.2	-12.6	.474	275	.272	4.58	-.1070	-.0114	-1.2534	-.0111	-.1010	-.0046
10	1	----------do----------	9	--------do---------	1	Full down	-----do-----	46	-.9	-3.9	-13.7	.400	240	.262	4.95	-.0876	-.0266	-1.4756	-.0080	-.1475	-.0001
11	1	----------do----------	9	--------do---------	2	2/3 up	1/3 with	25	5.3	2.6	-3.7	.619	366	.268	4.48	-.0787	.0344	-.9308	.0015	-.0528	-.0042
12	1	----------do----------	9	--------do---------	2	Full down	Full with	34	3.0	.7	-7.7	.584	321	.289	3.53	-.0804	-.0400	-1.2170	.0060	-.1247	-.0059
13	1	----------do----------	9	--------do---------	3	Full up	Full against	22	.8	-3.7	-6.9	.422	379	.176	11.24	-.0763	-.0108	-.8044	-.0103	-.0241	-.0027
14	1	----------do----------	9	--------do---------	3	Full down	-----do-----	24	-1.6	-5.4	-10.4	.482	353	.217	7.74	-.0854	.0419	-1.1376	-.0079	-.1193	-.0029
15	1	----------do----------	9	--------do---------	3	---do----	Neutral	22	-.1	-3.8	-8.4	.554	359	.244	6.59	-.0635	.0410	-1.0530	.0079	-.1109	-.0011
16	1	----------do----------	9	--------do---------	4	Neutral	Full against	24	-.5	-4.1	-10.1	.539	334	.256	6.19	-.0920	.0345	-.9902	-.0027	-.0691	-.0019
17	1	----------do----------	9	--------do---------	4	Full down	-----do-----	26	-.5	-4.6	-10.6	.482	314	.243	7.32	-.1037	.0342	-1.0883	.0009	-.1053	-.0034
18	1	----------do----------	9	Landing gear and flaps deflected 45°	1	Full up	-----do-----	48	-2.1	-5.8	-16.0	.350	209	.264	6.05	-.1577	.0023	-1.4608	-.0046	-.1118	-.0067
19	1	----------do----------	9	--------do---------	1	Full down	-----do-----	53	-1.7	-4.5	-18.3	.401	196	.322	3.81	-.1425	-.0244	-1.6697	-.0011	-.1804	-.0029
20	1	----------do----------	9	--------do---------	1	Neutral	Neutral	50	1.6	-1.6	-12.1	.365	209	.275	5.06	-.1280	-.0434	-1.5785	.0055	-.1493	-.0002
21	1	----------do----------	9	--------do---------	1	Full down	-----do-----	48	-2.3	-5.0	-19.7	.482	203	.375	3.10	-.1501	-.0163	-1.6536	.0051	-.1766	-.0042
22	1	----------do----------	9	Flaps deflected 45°	1	Full up	Full against	49	-3.2	-6.8	-15.5	.325	223	.230	6.78	-.1994	.0254	-1.4597	-.0003	-.1123	-.0089
23	1	----------do----------	9	--------do---------	1	Full down	-----do-----	52	-1.3	-4.2	-17.3	.393	197	.315	4.08	-.1438	-.0418	-1.6589	-.0026	-.1177	-.0024
24	1	----------do----------	9	--------do---------	1	Neutral	Neutral	45	.1	-2.9	-14.9	.403	197	.322	4.05	-.1414	-.0335	-1.5636	.0024	-.1410	-.0019
25	2 and 4	Small anti-spin fillets added to tail, fin and rudder extended up	10 and 11	Clean	1	Full up	Full against	55	-.3	-3.2	-13.0	.321	216	.235	5.46	-.0477	-.0030	-1.4334	.0010	-.1104	-.0158
26	3	Large anti-spin fillets added to tail	10	--------do---------	1	---do----	-----do-----	46	-3.1	-6.7	-16.0	.349	223	.247	6.51	-.0823	.0297	-1.3112	-.0013	-.0856	-.0146
27	3	----------do----------	10	--------do---------	1	---do----	2/3 against	50	2.0	-3.0	-5.2	.226	220	.162	13.50	-.0529	-.0455	-1.3398	-.0096	-.0967	-.0068
28	4	Fin and rudder extended upwards	11	--------do---------	1	---do----	Full against	64	1.6	-.3	-14.3	.384	197	.307	2.70	-.0198	-.0787	-1.4940	.0001	-.1399	-.0130
29	5	Fixed area added above fin and rudder	11	--------do---------	1	Neutral	-----do-----	67	.6	-1.2	-16.1	.378	190	.313	2.48	.0102	-.0871	-1.6125	.0044	-.1793	-.0131
30	6	Area added to front of fin	11	--------do---------	1	Full up	-----do-----	66	1.3	-.5	-13.7	.346	206	.264	3.02	-.0009	-.0639	-1.6095	.0020	-.1549	-.0182
31	7	Two ventral fins set at 45° on fuselage	12	--------do---------	1	Neutral	-----do-----	41	-2.1	-4.8	-12.9	.433	288	.237	4.99	-.0673	-.0058	-1.2608	-.0029	-.1073	-.0036
32	7	----------do----------	12	--------do---------	1	Full down	-----do-----	45	-4.4	-7.2	-19.4	.481	229	.331	3.64	-.0690	.0106	-1.4056	-.0032	-.1445	.0077

[a]Figure in which modification is shown.

NACA

TABLE IV.- TAIL-DAMPING POWER FACTORS FOR THE VARIOUS TAIL CONFIGURATIONS TESTED ON A FIGHTER MODEL

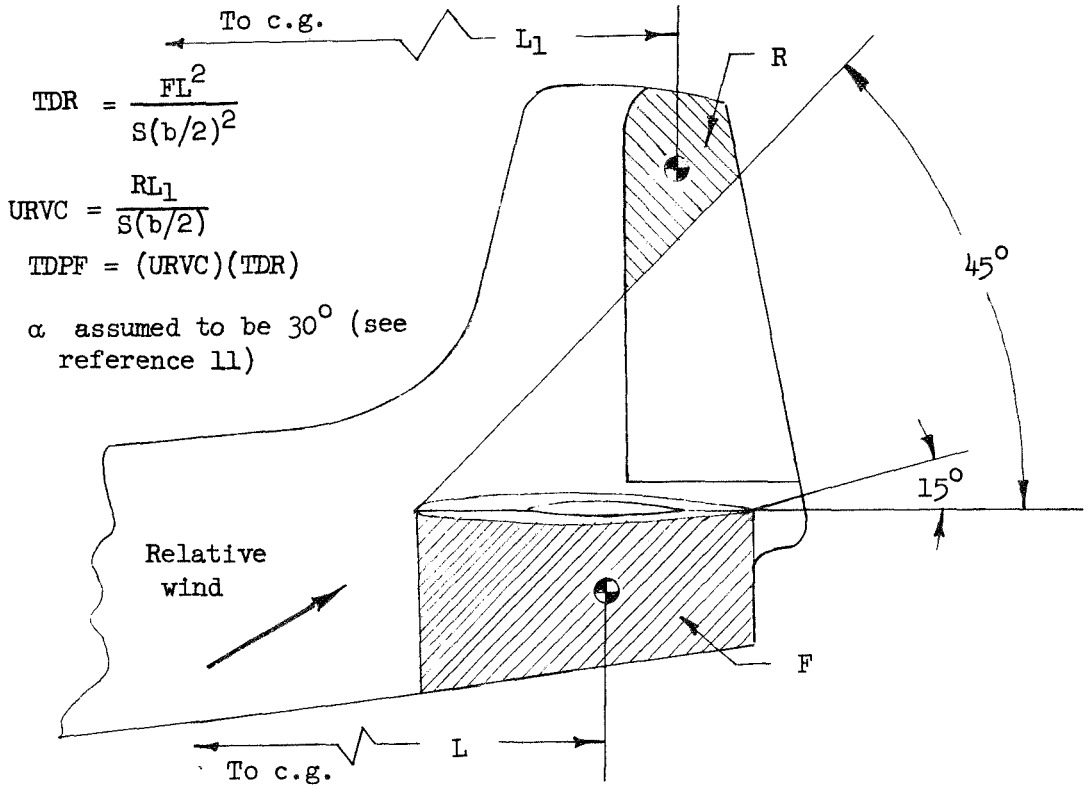

Modification	Figure (a)	Unshielded rudder volume coefficient, URVC (b)	Tail-damping ratio, TDR (b)	Tail-damping power factor, TDPF (b)
None		0.00948	0.0292	0.000277
1	9	.01500	.0243	.000364
2	10	.00948	.0454	.000431
3	10	.00948	.0464	.000440
4	11	.01870	.0292	.000546
5	11	.00948	.0292	.000277
6	11	.00948	.0292	.000277
7	12	.00948	.0288	.000273

[a]Figure in which modification is shown.

[b]Value as computed by methods of reference 11.

TABLE V.- COMPARISON OF APPROXIMATE SPIN RADII AND SIDESLIP ANGLES TESTED AND SPIN RADII AND SIDESLIP ANGLES CALCULATED FROM MEASURED AERODYNAMIC FORCES

Test	R_s (ft)	R_s (ft) (a)	ψ (a)	β_{cg}	β_{cg} (a)	Angles between the Z body axis and resultant force (a)	
						Angle in XZ-plane	Angle in YZ-plane
1	8.53	7.57	0	-5.2	-4.8	3.1	1.7
2	2.69	2.24	-4.9	-1.4	-1.0	.9	2.3
3	8.08	4.61	0	-6.5	-6.1	1.9	1.2
4	5.27	2.37	0	-6.1	-5.0	2.8	1.1
5	2.71	2.58	0	-.2	-.1	2.1	2.2
6	9.18	4.64	0	-4.4	-2.0	3.6	0
7	3.44	2.11	-5.0	-1.0	-.1	.7	2.0
8	6.62	3.30	-1.7	-3.4	-1.5	4.5	1.3
9	4.58	4.95	0	-4.2	-4.5	4.9	.5
10	4.95	5.80	0	-3.9	-4.4	3.4	1.0
11	4.48	3.16	3.1	2.6	3.4	4.8	2.1
12	3.53	3.59	-3.0	.7	-.6	3.8	1.9
13	11.24	6.92	0	-3.7	-2.0	5.4	.8
14	7.74	6.99	2.6	-5.4	-5.0	4.3	2.1
15	6.59	4.99	2.8	-3.8	-2.9	3.5	2.2
16	6.19	4.77	2.2	-4.1	-3.3	5.3	2.0
17	7.32	5.72	2.7	-4.6	-3.7	5.4	1.8
18	6.05	3.66	0	-5.8	-4.3	6.2	.1
19	3.81	2.84	-3.3	-4.5	-3.8	4.9	.8
20	5.06	4.38	-3.9	-1.6	-1.2	4.6	1.6
21	3.10	2.44	0	-5.0	-4.4	5.2	.5
22	6.78	6.47	2.3	-6.8	-6.6	7.6	1.0
23	4.08	3.00	-3.1	-4.2	-3.5	4.9	1.5
24	4.05	2.10	-2.8	-2.9	-1.4	5.2	1.2
25	5.46	5.09	0	-3.2	-3.0	1.9	.1
26	6.51	3.97	0	-6.7	-5.3	3.6	1.3
27	13.50	9.28	-3.7	-3.0	-1.4	2.3	2.0
28	2.70	1.43	-6.7	-.3	-.6	.8	3.0
29	2.48	1.55	-6.3	-1.2	-.5	.4	3.1
30	3.02	4.72	-2.8	-.5	-1.6	0	2.3
31	4.99	6.85	-1.7	-4.8	-5.8	3.1	.3
32	3.64	3.10	0	-7.2	-6.7	2.8	.4

[a]Values based on the measured aerodynamic forces.

NACA

TABLE VI.- THE EFFECT OF RUDDER REVERSAL ON THE NUMBER OF TURNS FOR RECOVERY AND ON THE AERODYNAMIC FORCE AND MOMENT COEFFICIENTS OF A FIGHTER MODEL IN A SPIN

[Coefficient increments obtained by setting the rudder from full with to full against the spin; recoveries attempted by rapid full rudder reversal except as indicated]

Test	$\frac{1}{10}$-scale model						$\frac{1}{20}$-scale model
	ΔC_X	ΔC_Y	ΔC_Z	ΔC_l	ΔC_m	ΔC_n	Turns for recovery
1	-0.0016	-0.0059	-0.002	0.0015	-0.0011	0.0028	>10
2	.0068	-.0001	.010	.0007	-.0054	-.0014	>11
3	.0031	.0013	-.012	.0022	-.0036	.0031	>9
4	-.0005	.0048	-.018	.0022	-.0046	-.0027	>8
5	.0019	.0118	.012	.0003	-.0001	-.0007	>4
6	.0021	-.0038	-.033	.0010	-.0029	-.0030	$1\frac{1}{4}$, $1\frac{1}{2}$
7	.0097	0	.006	.0008	-.0078	-.0009	>2, >$2\frac{3}{4}$
8	.0048	.0148	-.011	.0017	-.0014	-.0047	$1\frac{1}{2}$, $1\frac{3}{4}$
9	.0036	.0100	.014	.0012	-.0026	-.0055	2, $2\frac{1}{4}$
10	-.0035	.0165	.015	.0013	-.0018	-.0053	4
11	-.0070	.0290	.017	.0004	.0052	-.0119	>3, >$3\frac{3}{4}$, [a] $1\frac{1}{4}$, [a] $1\frac{3}{4}$
12	-.0071	.0226	-.032	.0031	-.0030	-.0069	$2\frac{3}{4}$
13	-.0066	.0330	.045	.0018	.0062	-.0120	$\frac{1}{4}$
14	-.0054	.0478	.016	.0031	.0084	-.0179	$1\frac{1}{2}$, 2
15	-.0090	.0501	.020	.0020	.0067	-.0196	$1\frac{1}{4}$
16	-.0102	.0422	.029	.0013	.0121	-.0166	1, 1
17	0	.0432	.038	.0028	.0089	-.0161	$1\frac{1}{2}$, $2\frac{3}{4}$
18	.0002	-.0034	-.010	.0042	-.0004	.0038	>11
19	.0065	.0012	-.006	.0002	-.0052	-.0024	>14
20	.0021	.0049	.023	.0014	-.0077	-.0021	6, 6
21	.0004	.0115	-.058	.0013	-.0088	-.0040	8
22	.0084	-.0070	.023	.0033	-.0001	-.0008	>$8\frac{3}{4}$
23	.0153	.0066	-.003	.0008	-.0003	-.0030	>9
24	.0069	.0092	-.034	.0022	-.0070	-.0032	>10
25	.0015	-.0031	.008	.0003	.0018	.0003	>3
26	0	-.0010	.010	.0003	.0008	.0032	>8
27	0	-.0021	-.006	.0007	-.0006	.0017	>10
28	.0011	.0024	.011	.0011	-.0003	-.0043	>5
29	.0004	-.0005	-.019	.0004	-.0038	-.0012	>13
30	.0009	-.0006	.083	.0007	.0020	.0009	>5
31	.0052	.0006	-.025	.0011	-.0084	-.0011	2, $2\frac{1}{4}$
32	.0015	-.0058	.012	.0015	-.0070	-.0018	>10

[a]Recovery attempted by simultaneous reversal of rudder from full with to 2/3 against the spin and elevator from 2/3 up to 1/3 down.

NACA

TABLE VII.- THE EFFECT OF UNSHIELDING THE VERTICAL TAIL BY HORIZONTAL-TAIL MOVEMENT ON THE AERODYNAMIC FORCE AND MOMENT COEFFICIENTS OF A FIGHTER MODEL IN A SPIN

[Coefficient increments obtained by moving the horizontal tail 15 in. (full-scale) rearward from the original position; rudder full with the spin]

Test	ΔC_X	ΔC_Y	ΔC_Z	ΔC_l	ΔC_m	ΔC_n
1	-0.0016	-0.0176	0.018	-0.0162	-0.0018	0.0005
3	-.0064	.0037	.010	-.0026	-.0040	.0007
25	-.0990	.0053	-.045	-.0020	-.0130	.0036
26	-.0300	.0004	-.022	-.0027	-.0046	.0041
27	-.0102	.0017	-.019	-.0011	-.0094	.0020
28	-.0240	.0069	-.074	-.0017	-.0189	.0025
29	-.0210	.0198	-.026	-.0021	-.0155	-.0039
30	-.0264	.0164	.053	.0035	-.0067	.0035
31	-.0189	.0077	-.070	-.0028	-.0128	-.0039
32	-.0415	.0208	-.058	.0038	-.0096	-.0069

NACA

TABLE VIII.- THE EFFECT OF UNSHIELDING THE VERTICAL TAIL ON RUDDER-REVERSAL EFFECTIVENESS ON A FIGHTER MODEL IN A SPIN

[Coefficient increments obtained by reversing the rudder from full with to full against the spin]

Test	Horizontal tail in original position		Horizontal tail in rearward position	
	ΔC_Y	ΔC_n	ΔC_Y	ΔC_n
1	-0.0059	0.0028	0.0083	-0.0031
3	.0013	.0031	.0123	-.0040
25	-.0031	.0003	0	-.0016
26	-.0010	.0032	.0012	-.0006
27	-.0021	.0017	.0009	.0003
28	.0024	-.0043	.0233	-.0088
29	-.0005	-.0012	.0053	-.0037
30	-.0006	.0009	.0066	-.0024
31	.0006	-.0011	.0107	-.0053
32	-.0058	-.0018	.0171	-.0027

NACA

TABLE IX.- EFFECT OF LANDING FLAPS ON THE YAWING-MOMENT-COEFFICIENT INCREMENTS DUE TO SETTING THE RUDDER FROM FULL WITH TO FULL AGAINST THE SPIN ON A FIGHTER MODEL

[Horizontal tail moved 15 in. rearward (full-scale)]

Elevator deflection	Aileron deflection	$\frac{1}{20}$-scale-model free-spinning results			$\frac{1}{10}$-scale-model aerodynamic yawing-moment coefficient					
					Flaps neutral			Flaps 45° down		
		α (deg)	ϕ (deg)	$\frac{\Omega b}{2V}$	Rudder with	Rudder against	ΔC_n	Rudder with	Rudder against	ΔC_n
Full up	Full against	46	0.4	0.252	-0.0034	-0.0081	-0.0047	-0.0046	-0.0030	0.0016
Neutral	--do--	38	-1.4	.272	-.0046	-.0101	-.0055	.0030	0	-.0030
Full down	--do--	46	-.9	.262	-.0002	-.0055	-.0053	.0027	-.0006	-.0033
Full down	--do--	52	-1.3	.315	-.0041	-.0095	-.0054	-.0024	-.0054	-.0030
Full up	Neutral	25	5.3	.268	-.0075	-.0167	-.0092	-.0104	-.0132	-.0028
Neutral	Neutral	45	.1	.322	-.0074	-.0116	-.0042	-.0019	-.0051	-.0032
Full up	--do--	25	-3.2	.268	-.0090	-.0213	-.0123	-.0114	-.0164	-.0050
Full up	--do--	52	5.3	.315	-.0042	-.0077	-.0035	-.0079	-.0101	-.0022
Full up	--do--	52	-1.3	.315	-.0102	-.0147	-.0045	-.0109	-.0117	-.0008

TABLE X.- COMPARISON OF THE RESULTANT INERTIA AND AERODYNAMIC FORCE COEFFICIENTS AND OF THE INERTIA AND AERODYNAMIC MOMENT COEFFICIENTS OF A FIGHTER MODEL IN A SPIN

Run	α (deg)	ϕ (deg)	C_R			C_l			C_m			C_n		
			Inertia	Aerodynamic	Difference	Inertia	Aerodynamic	Difference	Inertia	Aerodynamic	Difference	Inertia	Aerodynamic	Difference
1	46	-1.4	1.321	1.249	0.072	0.0012	-0.0106	0.0094	0.0705	-0.0841	0.0136	0.0013	-0.0025	0.0012
2	63	.6	1.622	1.574	.048	-.0016	-.0011	.0027	.1479	-.1697	.0218	-.0009	-.0087	.0096
3	43	-3.6	1.654	1.330	.324	.0041	-.0106	.0065	.1009	-.1107	.0098	.0049	-.0051	.0002
4	42	-3.3	1.900	1.426	.474	.0065	-.0050	-.0015	.1758	-.1360	-.0398	.0079	-.0033	-.0046
5	50	2.0	1.472	1.447	.025	-.0059	-.0013	.0072	.2293	-.1076	-.1217	-.0055	-.0068	.0123
6	35	.5	1.656	1.174	.482	-.0005	.0075	-.0070	.0952	-.0895	-.0057	-.0008	-.0016	.0024
7	60	1.4	1.795	1.655	.140	-.0036	.0091	-.0055	.1534	-.1750	.0216	-.0023	-.0053	.0076
8	46	.4	1.671	1.340	.331	-.0006	-.0072	.0078	.1178	-.0881	-.0297	-.0006	-.0033	.0039
9	38	-1.4	1.205	1.258	-.053	.0020	-.0111	.0091	.1336	-.1010	-.0326	.0028	-.0046	.0018
10	46	-.9	1.354	1.480	-.126	.0014	-.0080	.0066	.1272	-.1475	.0203	.0015	-.0001	-.0014
11	25	5.3	1.030	.935	.095	-.0103	.0015	.0088	.0677	-.0528	-.0149	.0012	-.0042	.0030
12	34	3.0	1.088	1.220	-.132	-.0020	.0060	-.0040	.1073	-.1247	.0174	.0007	-.0059	.0052
13	22	.8	.957	.809	.148	-.0005	-.0103	.0108	.0116	-.0241	.0125	-.0003	-.0027	.0030
14	24	-1.6	1.048	1.142	-.094	.0015	-.0079	.0064	.0341	-.1193	.0852	.0009	-.0029	.0020
15	22	-.1	1.127	1.056	.071	.0001	.0079	-.0080	.0433	-.1109	.0676	.0001	-.0011	.0010
16	24	-.5	1.010	.995	.015	.0004	-.0027	.0023	.1000	-.0691	-.0309	.0001	-.0019	.0018
17	26	-.5	1.090	1.094	-.004	.0004	.0009	-.0013	.0957	-.1053	.0096	.0008	-.0034	.0026
18	48	-2.1	1.728	1.470	.258	.0034	-.0046	.0012	.1286	-.1118	-.0168	.0033	-.0067	.0034
19	53	-1.7	1.828	1.678	.150	.0044	-.0011	-.0033	.1848	-.1804	-.0044	.0036	-.0029	-.0007
20	50	1.6	1.676	1.586	.090	-.0029	.0055	-.0026	.1377	-.1493	.0116	-.0026	-.0002	.0028
21	48	-2.3	1.832	1.659	.173	.0075	.0051	-.0126	.2588	-.1766	-.0822	.0072	-.0042	-.0030
22	49	-3.2	1.495	1.475	.020	.0039	-.0003	-.0036	.0971	-.1123	.0152	.0038	-.0089	.0051
23	52	-1.3	1.835	1.666	.169	.0032	-.0026	-.0006	.1782	-.1177	-.0605	.0027	-.0024	-.0003
24	45	.1	2.045	1.571	.474	-.0002	.0024	-.0022	.1925	-.1410	-.0515	-.0003	-.0019	.0022
25	55	-.3	1.030	1.434	-.404	-.0004	.0010	-.0006	.0959	-.1104	.0145	.0003	-.0158	.0155
26	46	-3.1	1.468	1.315	.153	.0042	-.0013	-.0029	.1129	-.0856	-.0273	.0044	-.0146	.0102
27	50	2.0	1.568	1.342	.226	-.0012	-.0096	.0108	.0480	-.0967	.0487	-.0012	-.0068	.0080
28	64	1.6	1.513	1.496	.017	-.0042	.0001	.0041	.1378	-.1399	.0021	-.0022	-.0130	.0152
29	67	.6	1.512	1.614	-.102	-.0017	.0044	-.0027	.1326	-.1793	.0467	-.0008	-.0131	.0139
30	66	1.3	1.609	1.610	-.001	-.0026	.0020	.0006	.0955	-.1549	.0594	-.0012	-.0182	.0194
31	41	-2.1	1.688	1.264	.424	.0024	-.0029	.0005	.1032	-.1073	.0041	.0030	-.0036	.0006
32	45	-4.4	1.448	1.427	.021	.0105	-.0032	-.0073	.2023	-.1445	-.0578	.0115	-.0077	-.0038

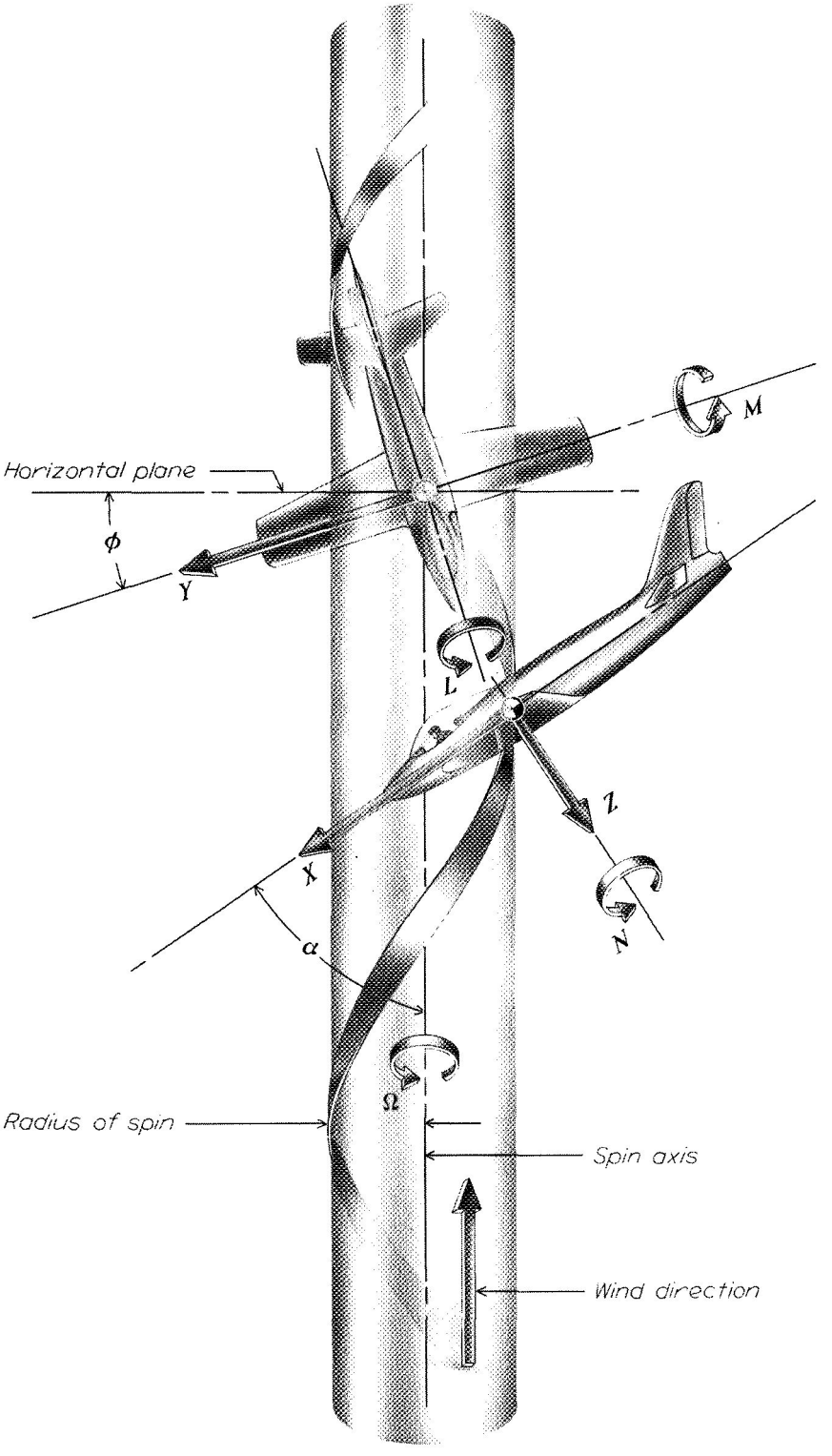

NACA
L-64907

Figure 1.- Illustration of an airplane in a steady spin. Arrows indicate positive directions of forces and moments along and about the body axes of the airplane.

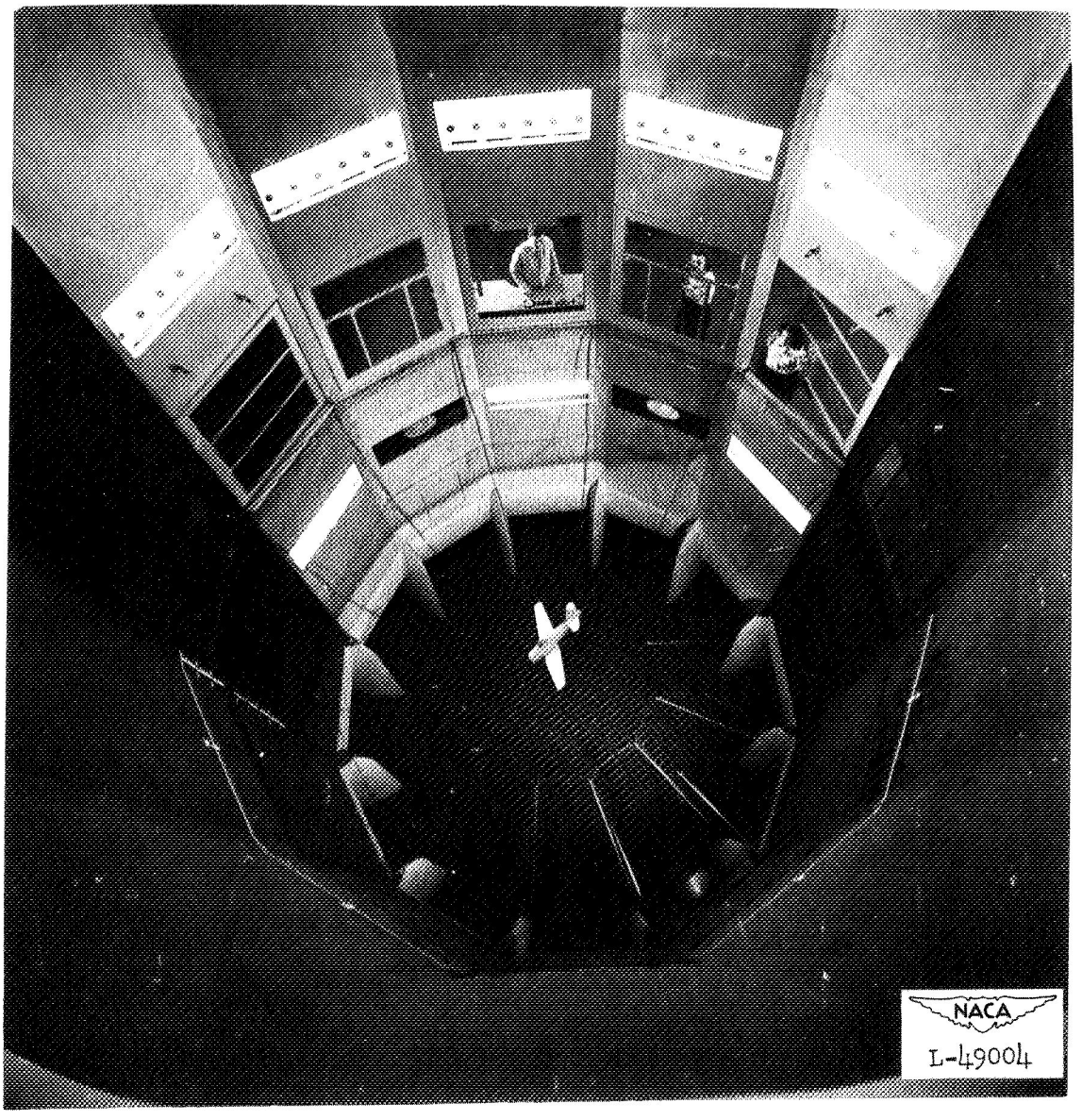

Figure 2.- The spinning model is supported in the tunnel by the vertically rising air current and the character of the spin is recorded by means of motion pictures. One of the three operators launches the model into the tunnel, a second operator controls the air speed and the third operates the camera.

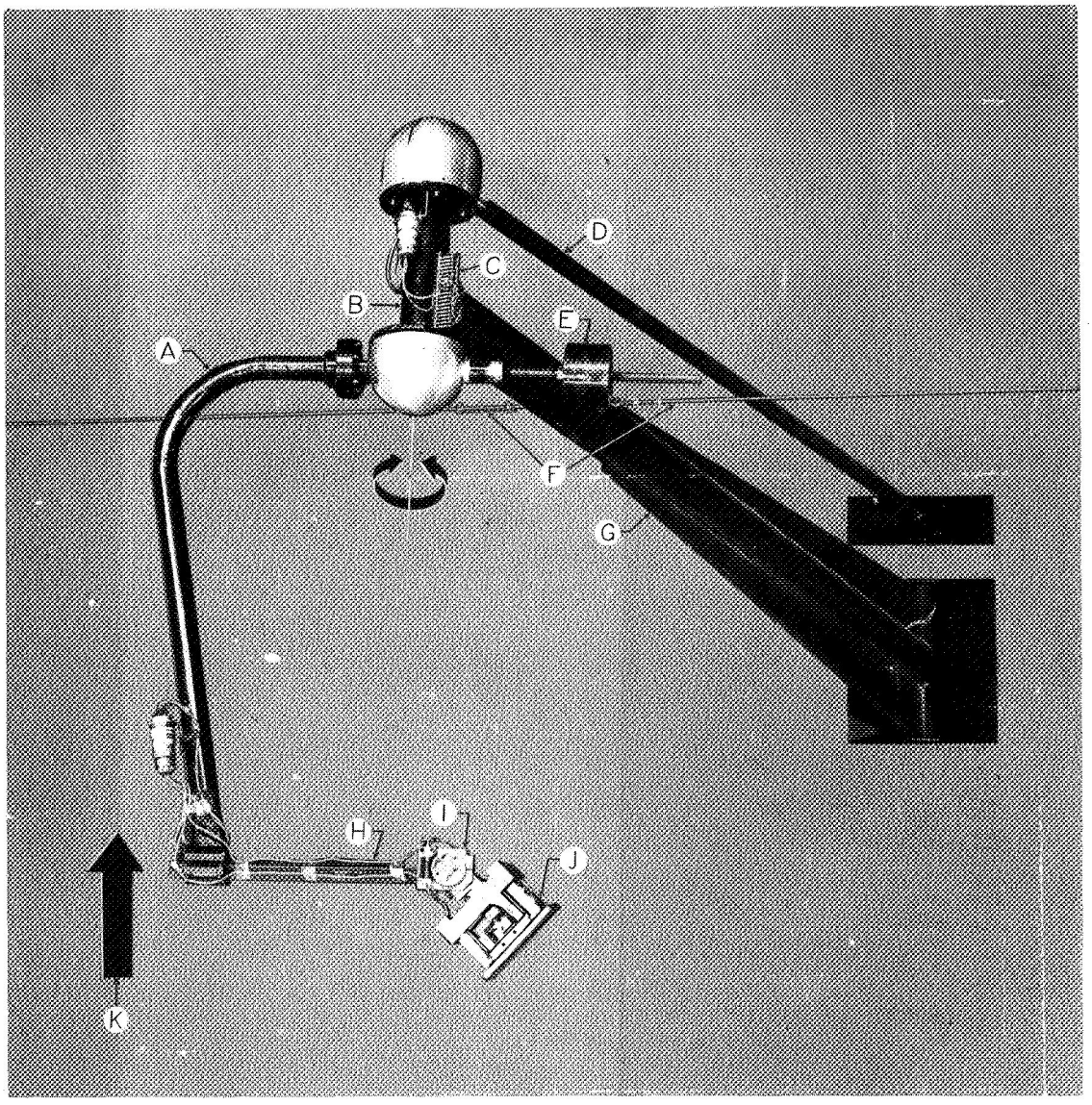

A	Rotary arm	F	Cables
B	Vertical member	G	Horizontal supporting arm
C	Slip rings and brushes	H	Spin-radius setting arm
D	Drive shaft	I	Model-attitude setting block
E	Counterweights	J	Strain-gage balance
		K	Wind direction

NACA

L-64905

Figure 3.- The rotary balance in the Langley 20-foot free-spinning tunnel.

72

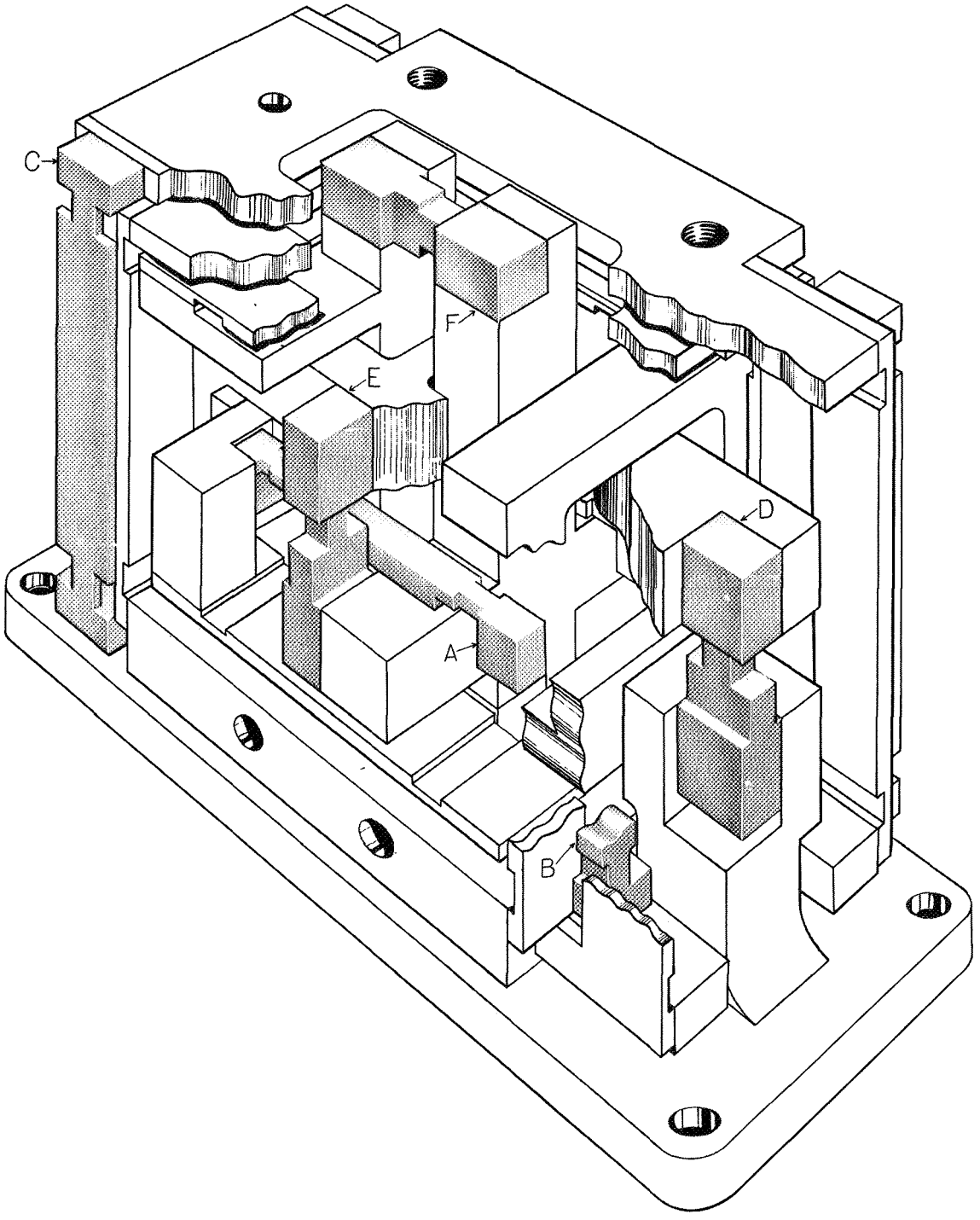

A Normal-force beam
B Longitudinal-force beam
C Lateral-force beam
D Rolling-moment beam
E Pitching-moment beam
F Yawing-moment beam

NACA
L-64906

Figure 4.- Illustration of the six-component strain-gage balance.

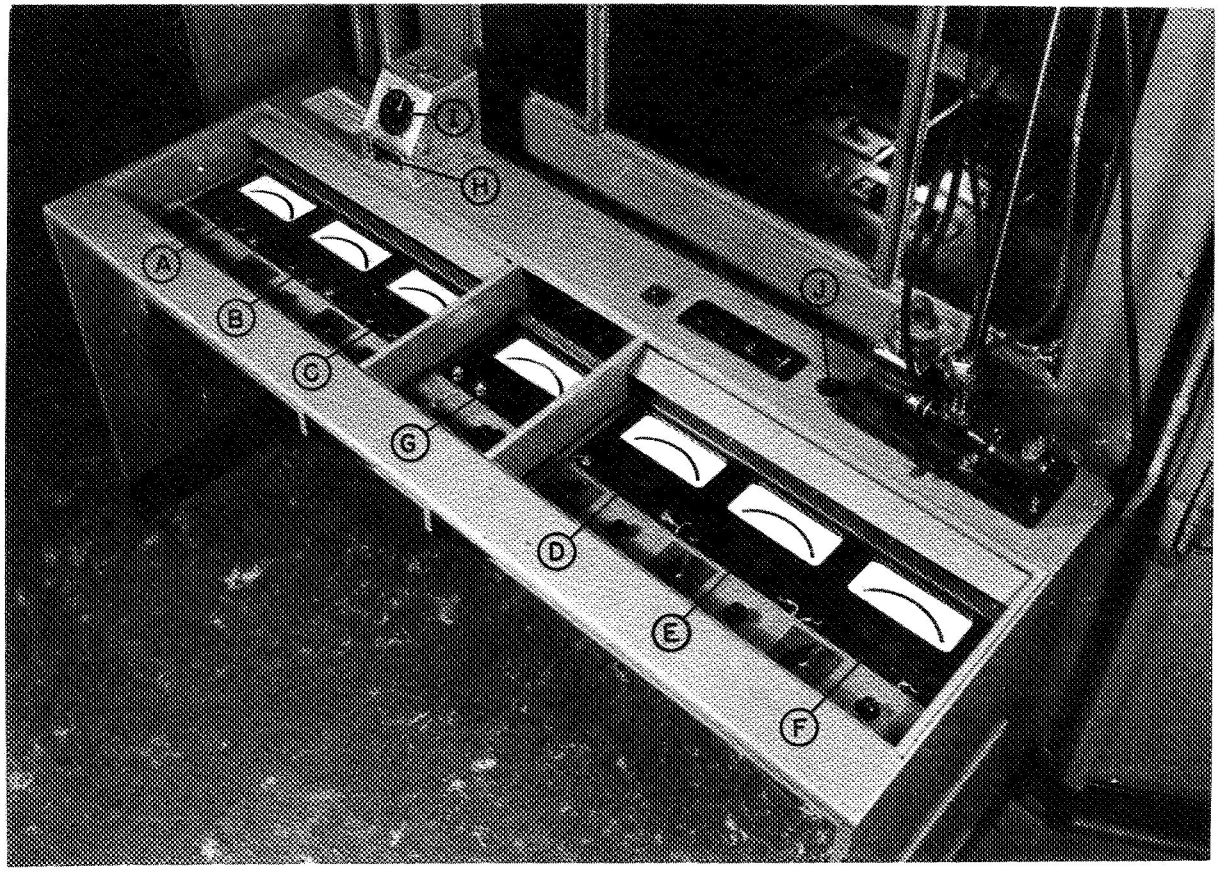

NACA L-54513.1

A	Normal-force meter	F	Yawing-moment meter
B	Longitudinal-force meter	G	Voltmeter
C	Lateral-force meter	H	Angular velocity regulator
D	Rolling-moment meter	I	Angular velocity indicator
E	Pitching-moment meter	J	Vertical descent velocity regulator

Figure 5.- The instrument panel of the rotary balance system for recording force and moment data.

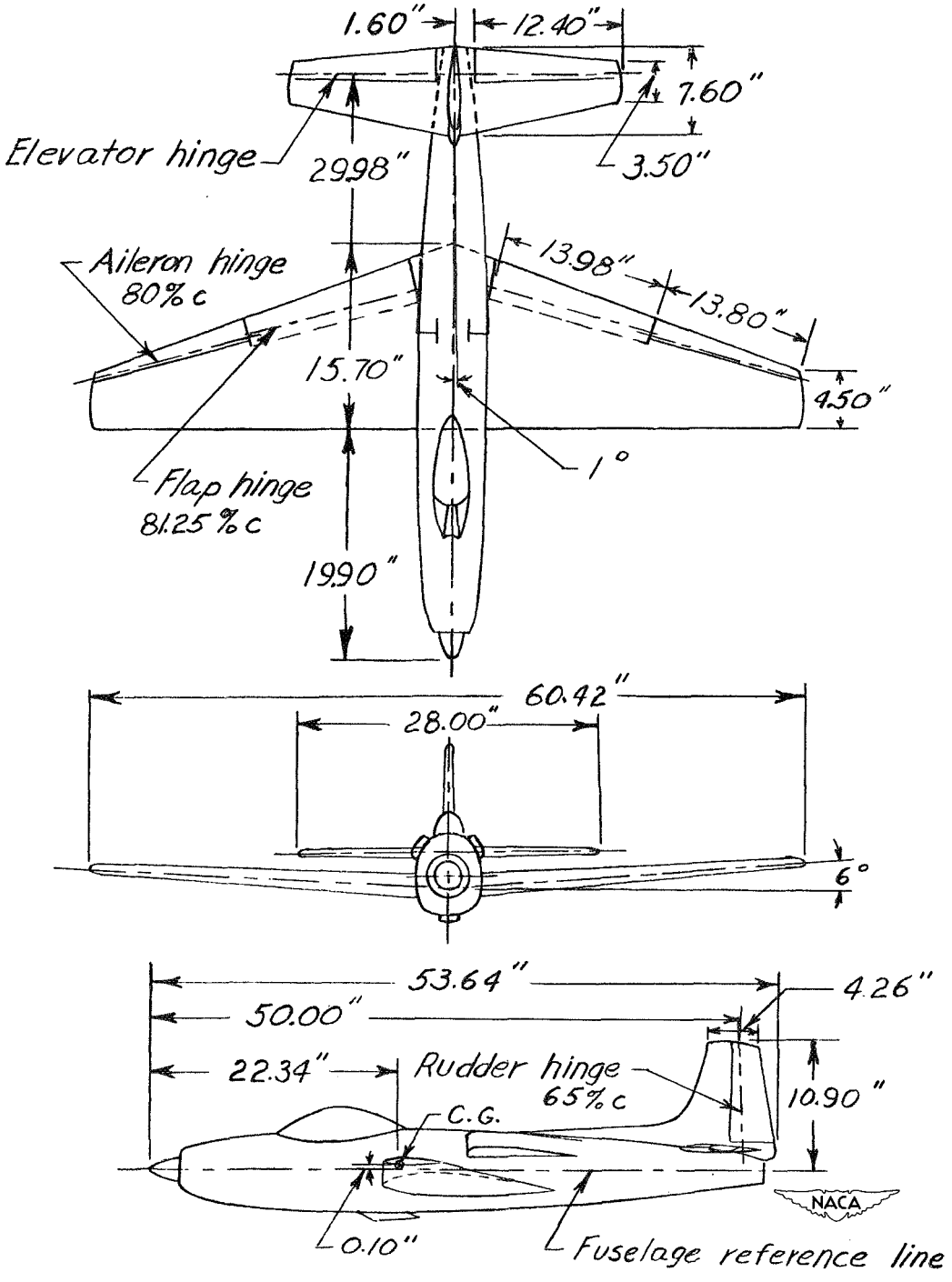

Figure 6.- Drawing of the $\frac{1}{10}$-scale model of a fighter airplane as tested on the rotary balance. Wing incidence, $2\frac{1}{2}^{\circ}$ leading edge up; stabilizer incidence, 1° leading edge up. Center-of-gravity position shown for normal loading.

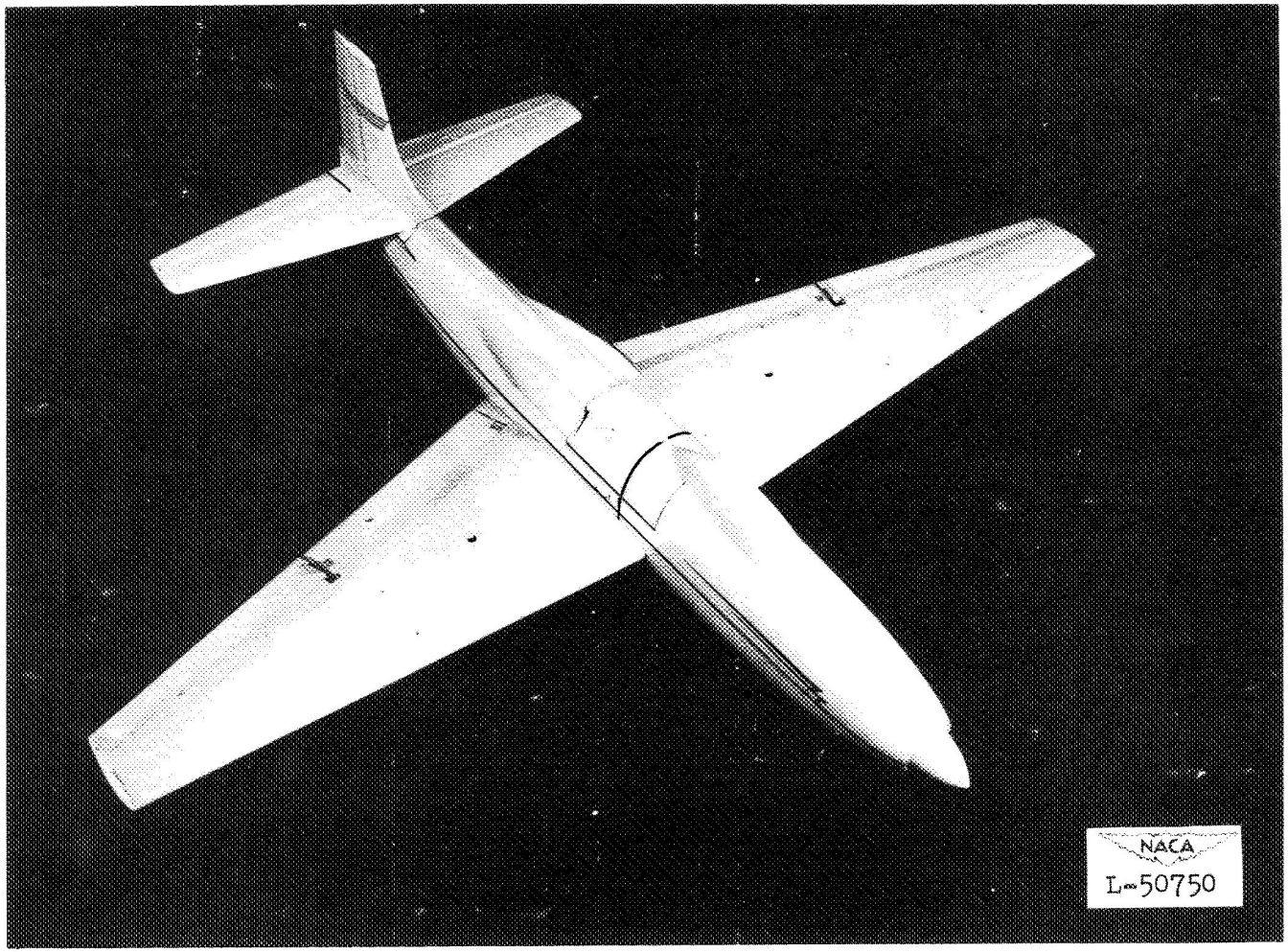

Figure 7.- The $\frac{1}{10}$-scale model of a fighter airplane in the clean condition.

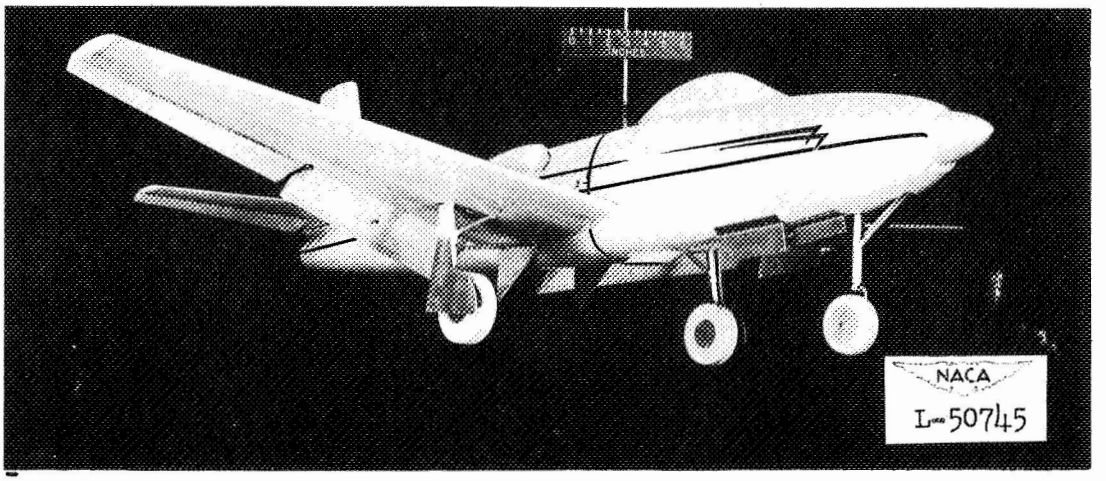

Landing condition

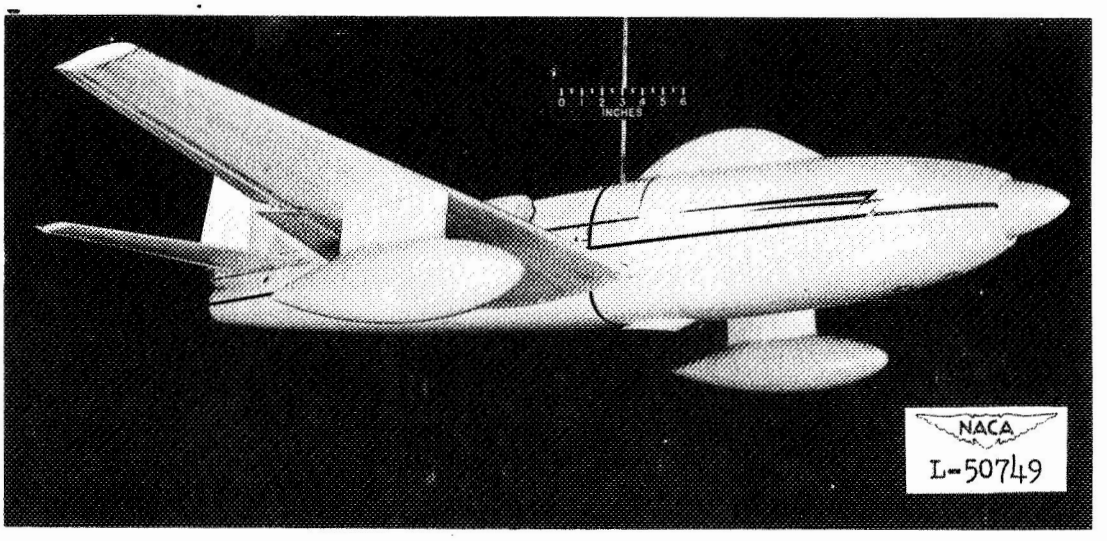

External wing fuel tanks installed

Figure 8.- The $\frac{1}{10}$-scale model of a fighter airplane in the landing condition and with external wing fuel tanks installed.

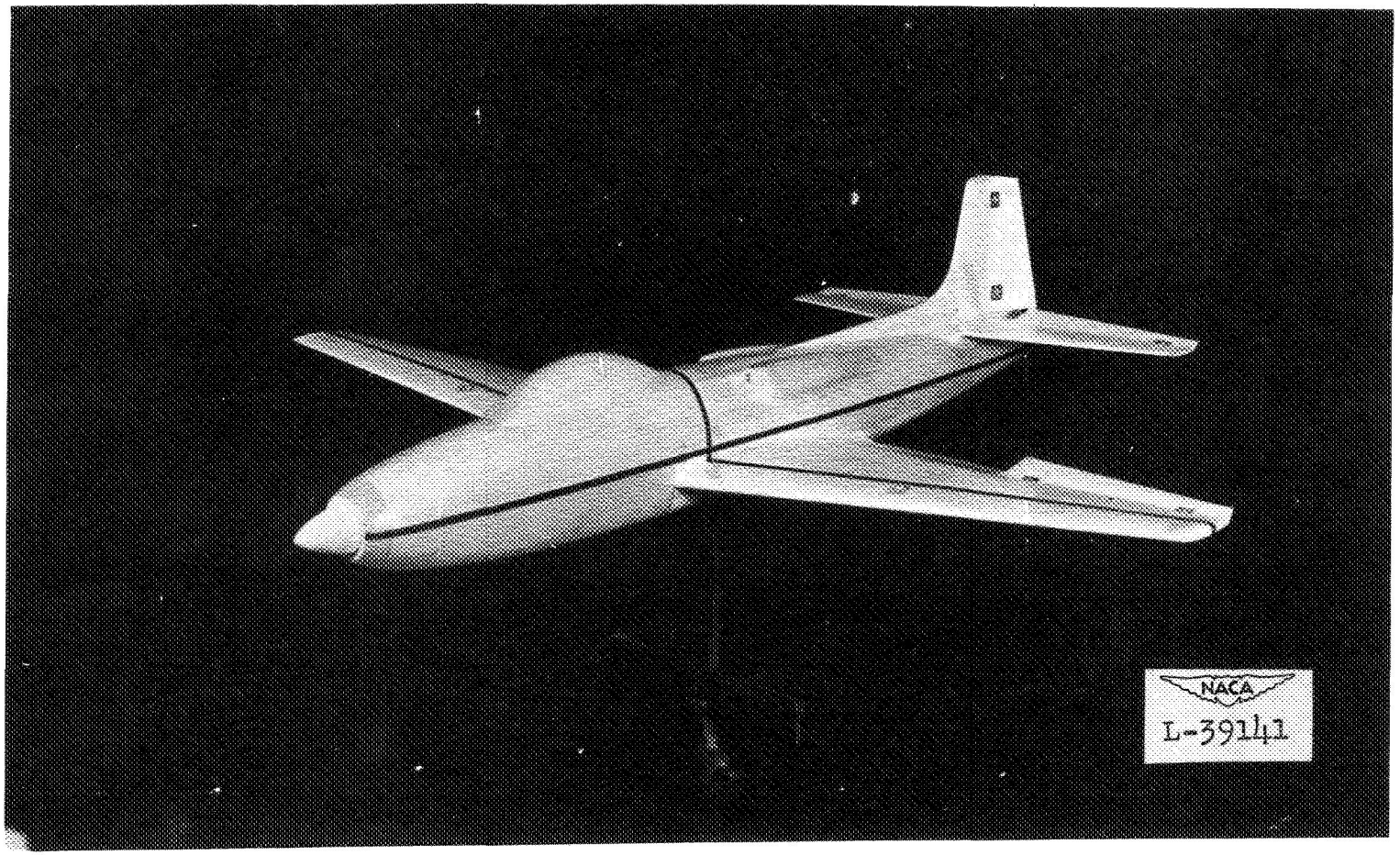

Figure 9.- The $\frac{1}{20}$-scale model of a fighter airplane in the clean condition.

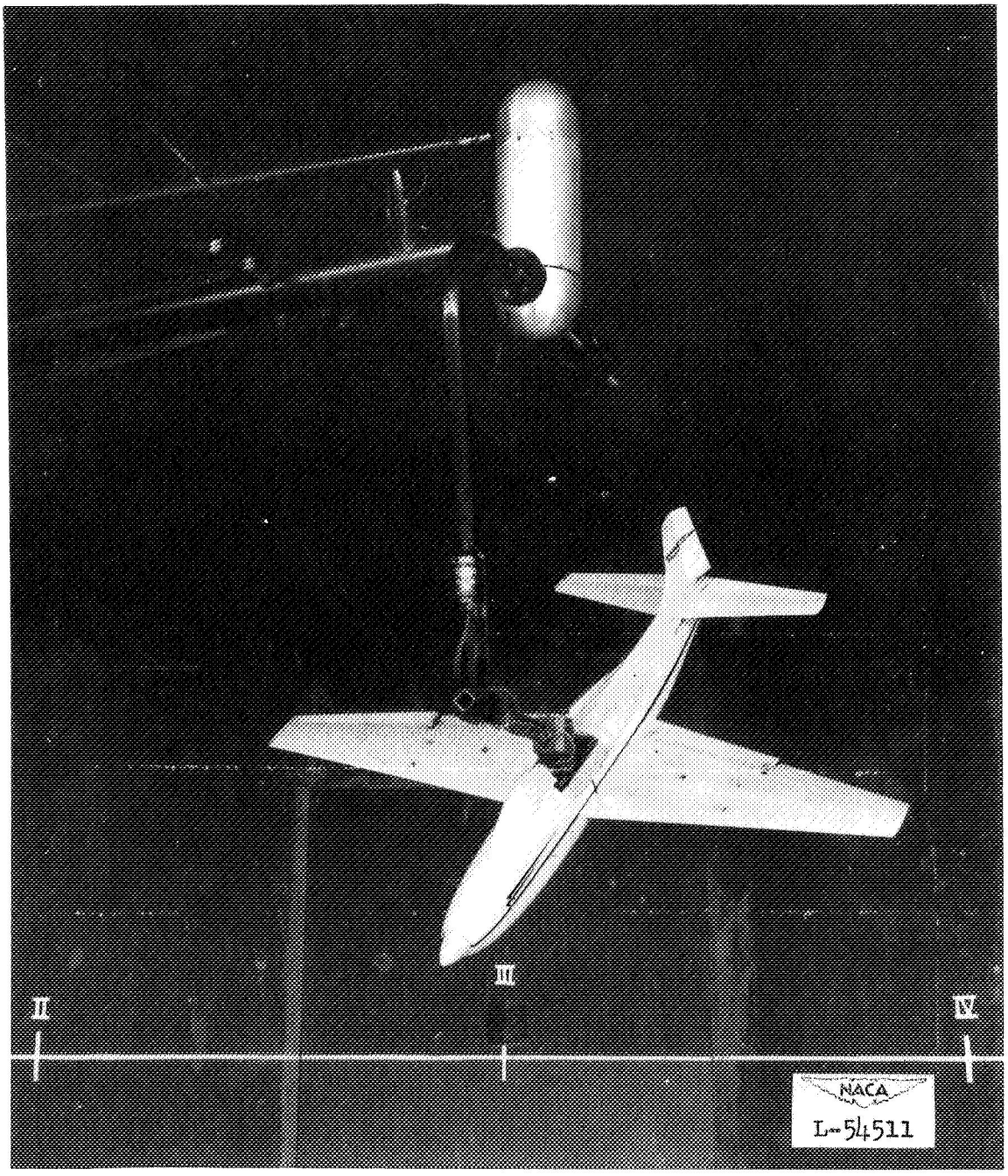

Figure 10.- The $\frac{1}{10}$- scale model of a fighter airplane mounted on the rotary balance in the Langley 20-foot free-spinning tunnel.

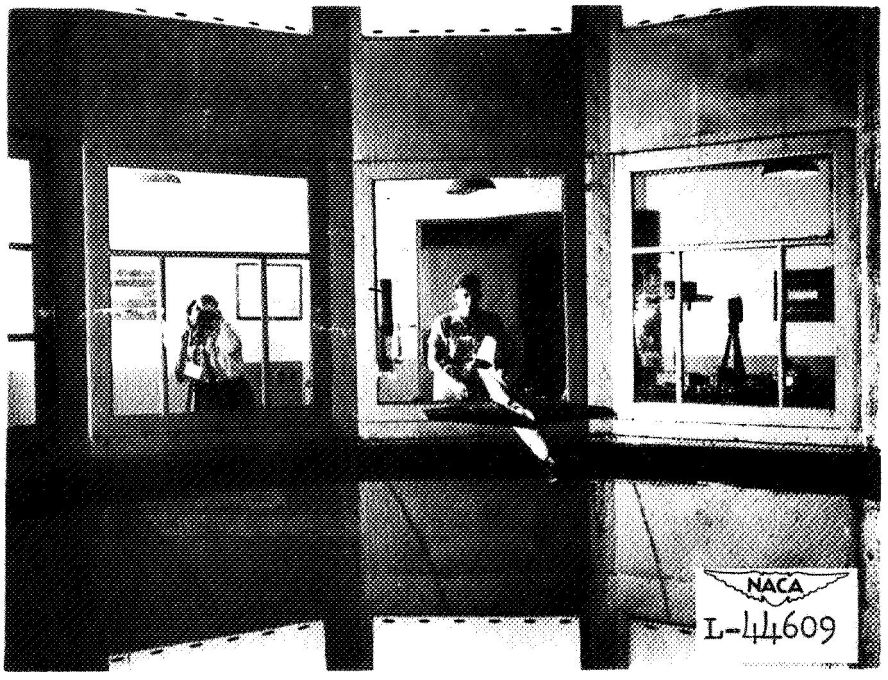

Figure 11.- Photograph of the $\frac{1}{20}$- scale model of a fighter airplane spinning in the Langley 20-foot free-spinning tunnel.

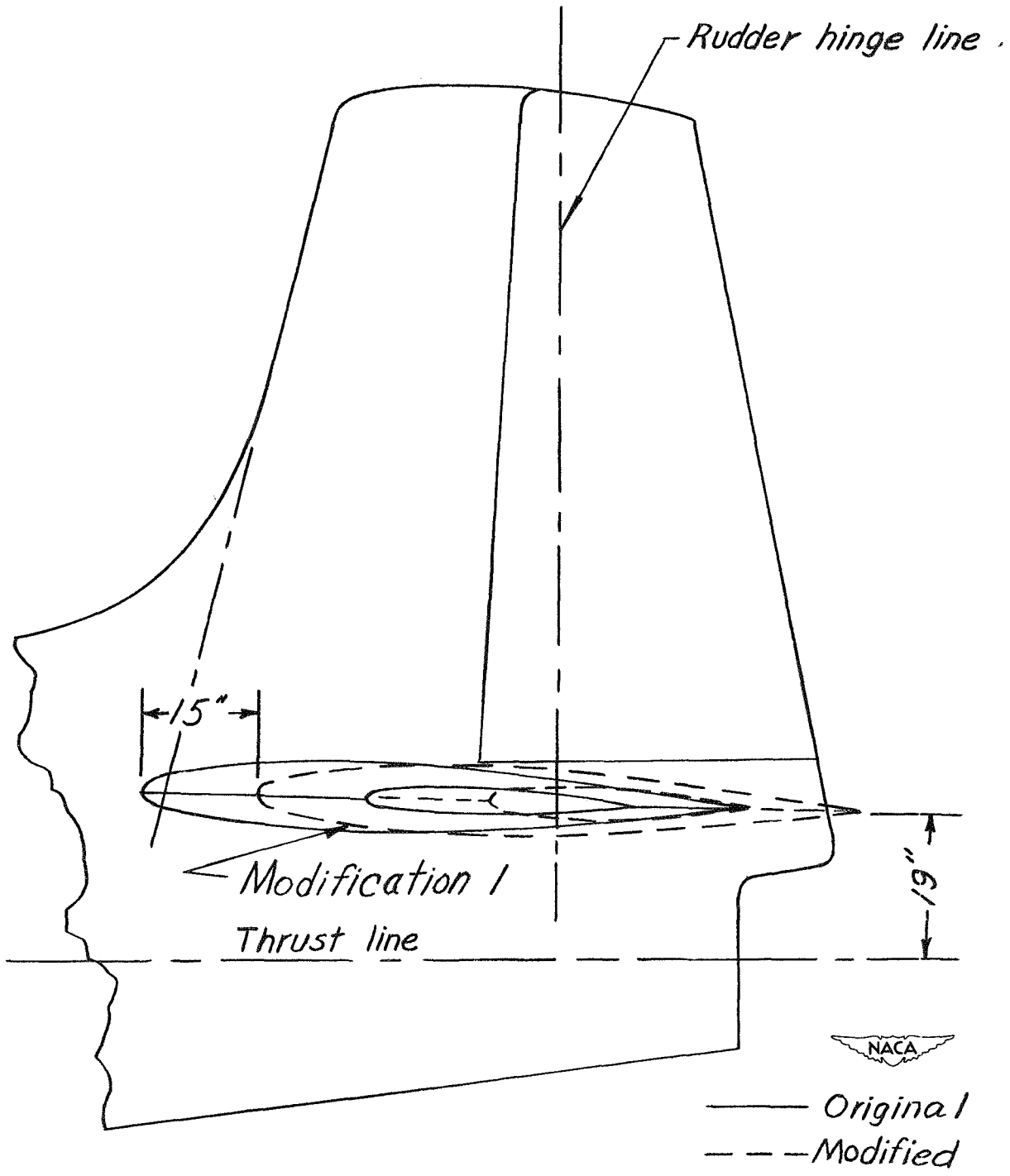

Figure 12.- Original and modified longitudinal positions of horizontal tail tested on the $\frac{1}{20}$- scale and $\frac{1}{10}$- scale models of a fighter airplane. Dimensions are full-scale.

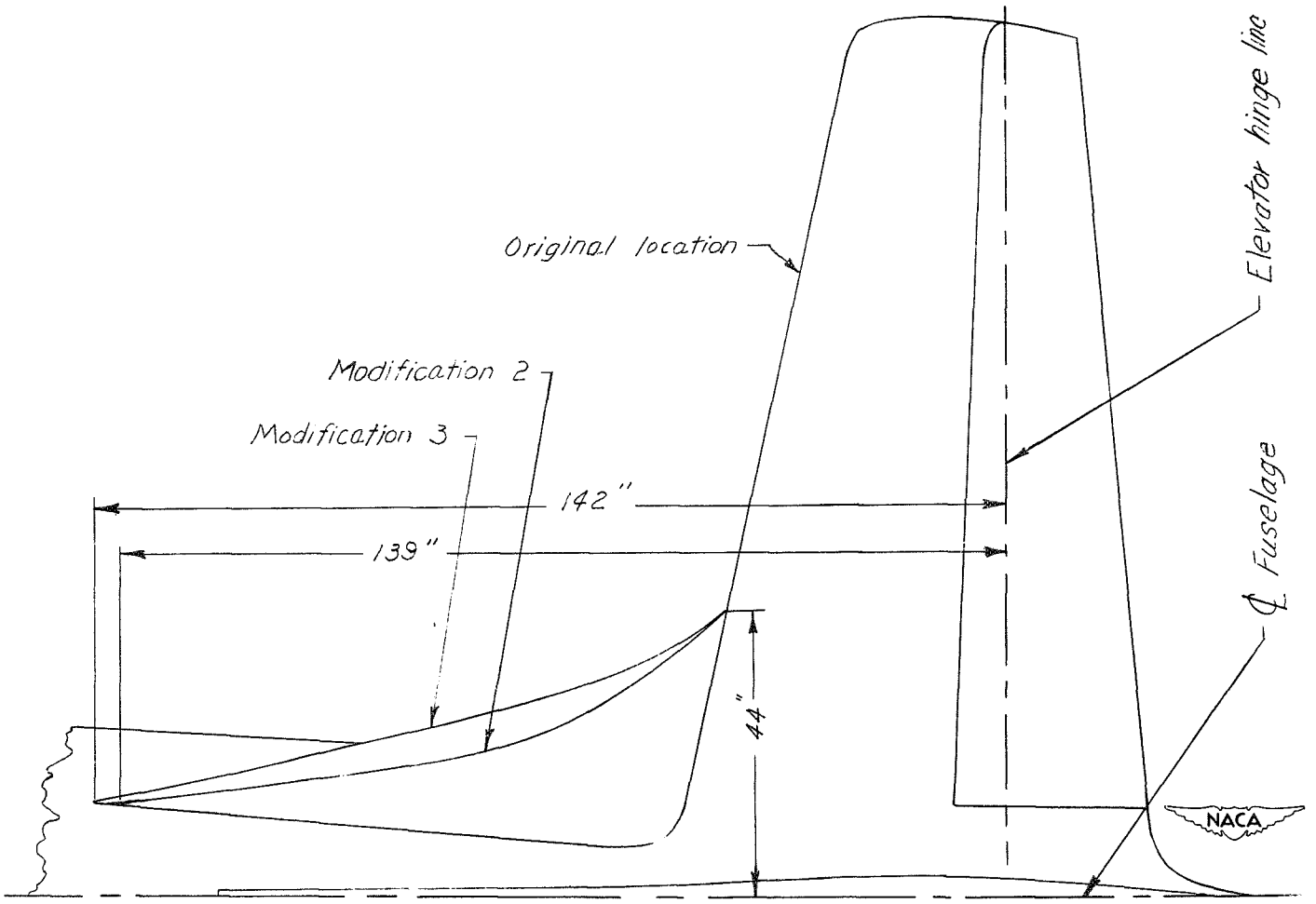

Figure 13 .- Original location of the horizontal tail tested and the anti-spin fillets tested on the $\frac{1}{20}$ - scale and $\frac{1}{10}$ - scale models of a fighter airplane. Dimensions are full-scale.

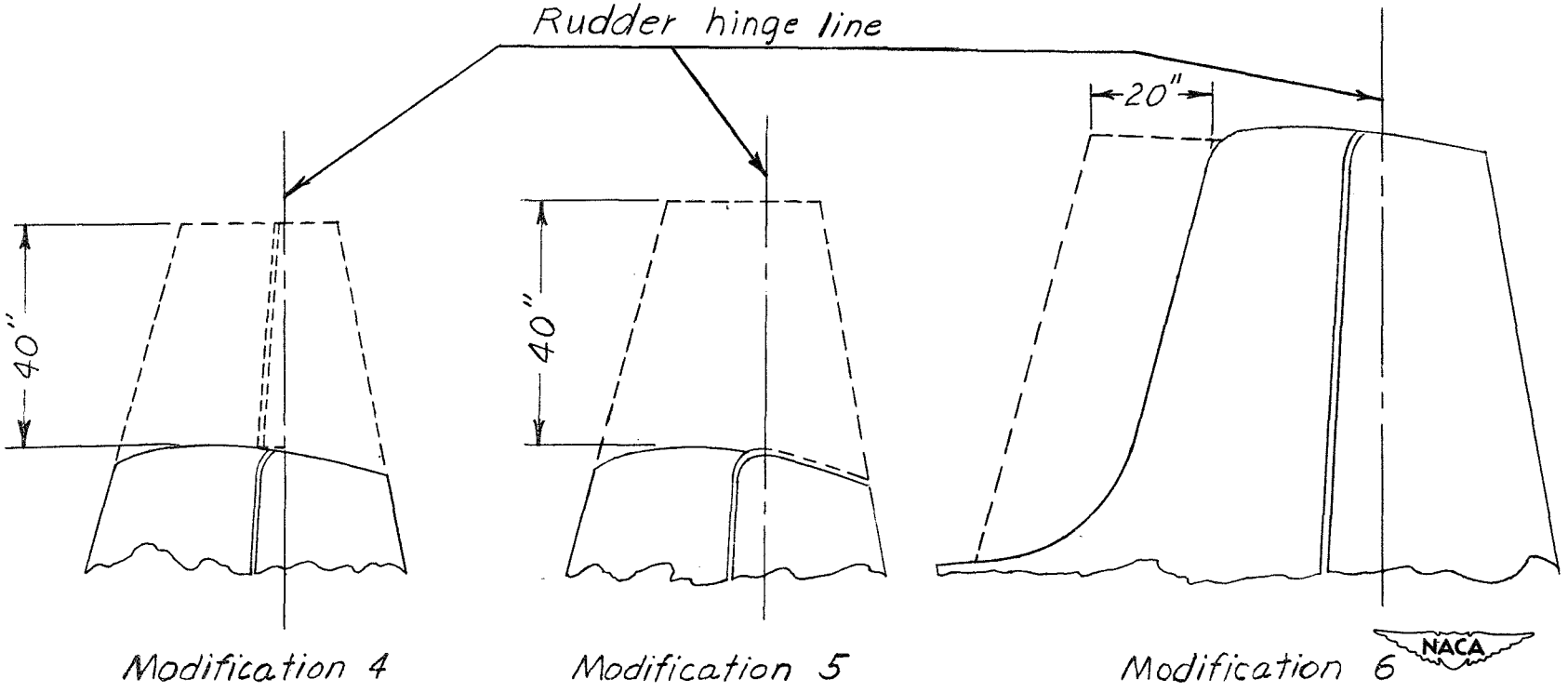

Figure 14.- Modifications to the vertical tail tested on the $\frac{1}{20}$ - scale and $\frac{1}{10}$ - scale models of a fighter airplane. Dimensions are full-scale.

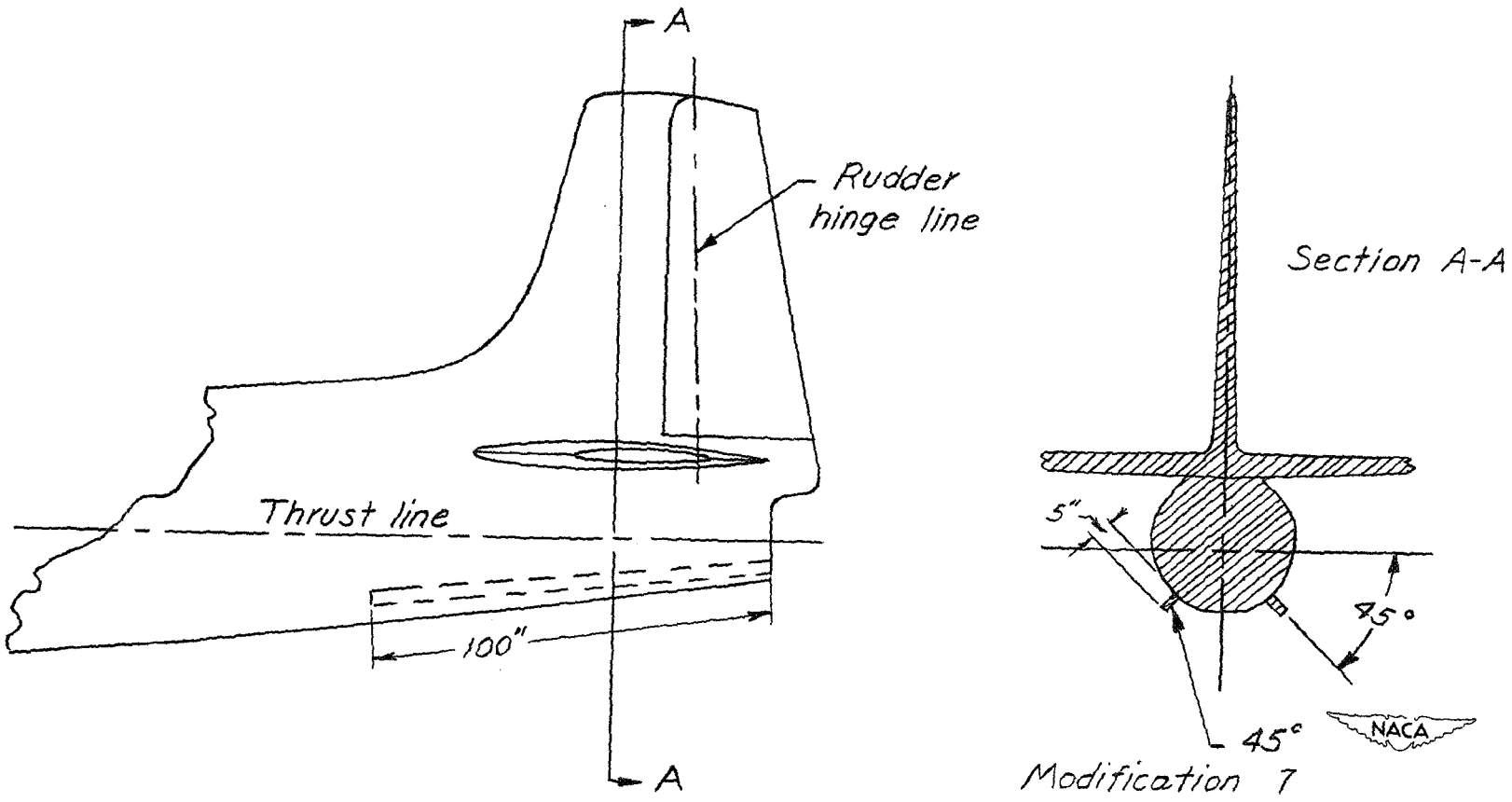

Figure 15.- Ventral fins tested on the $\frac{1}{20}$-scale and $\frac{1}{10}$-scale models of a fighter airplane. Dimensions are full-scale.

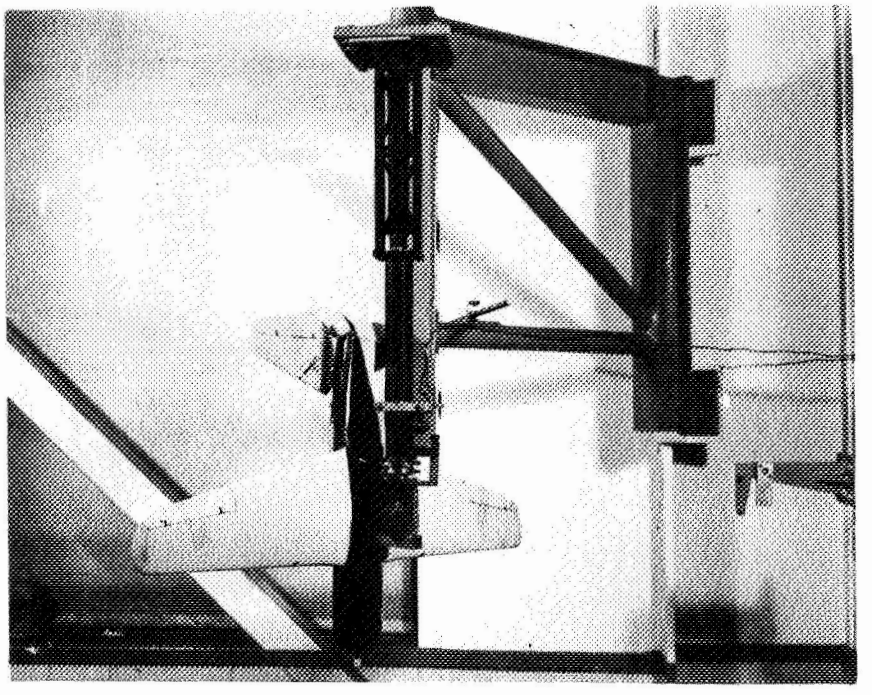

(a) Moment-of-inertia gear. NACA L-50754

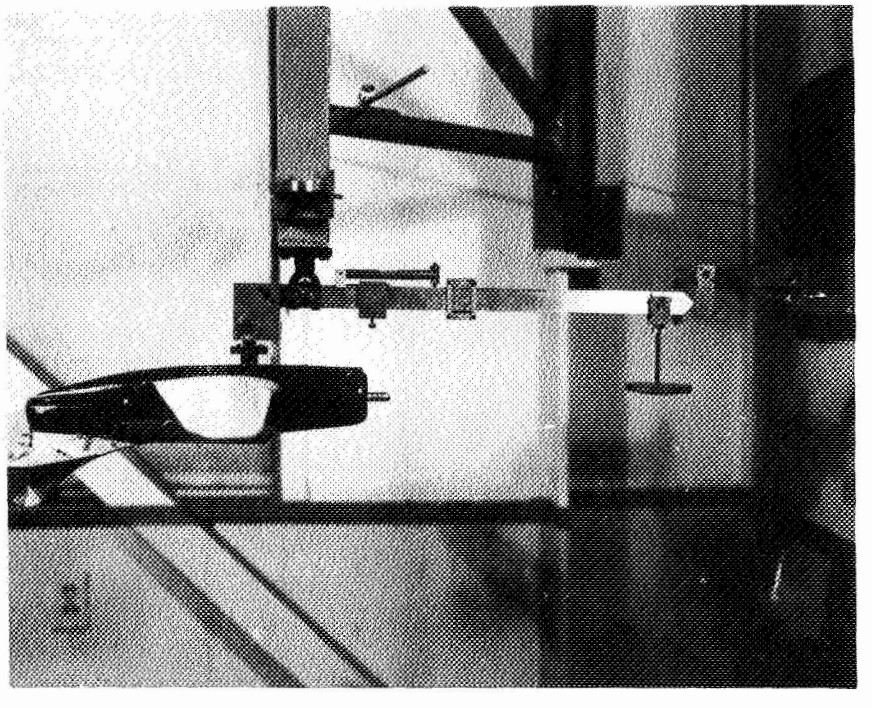

(b) Center-of-gravity gear. NACA L-50759

Figure 16.- Moment-of-inertia and center-of-gravity gear.

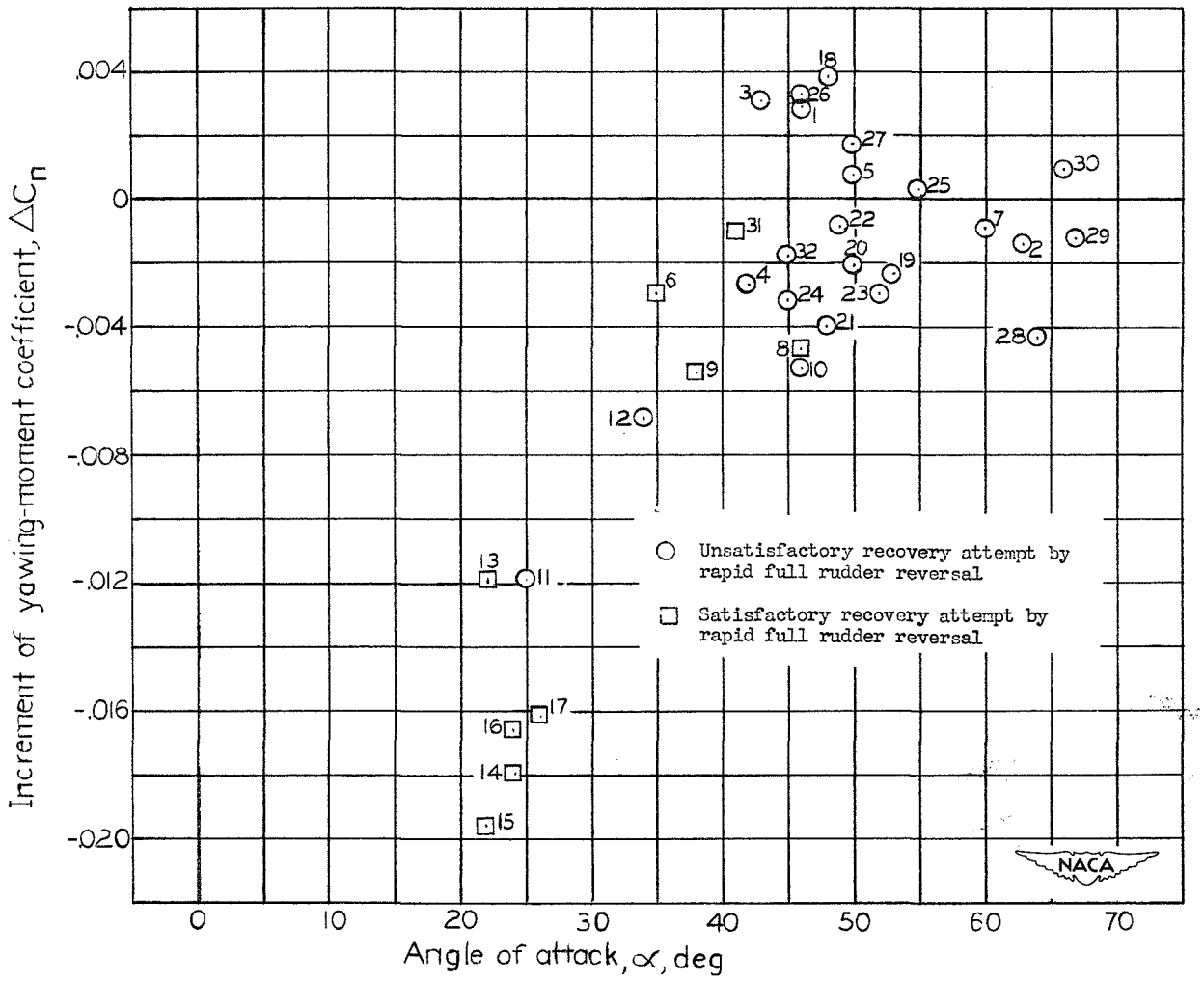

Figure 17.- Variation of the increment of yawing-moment coefficient caused by rudder reversal with angle of attack for spins of a model of a fighter airplane. Numbers refer to test conditions in table III.

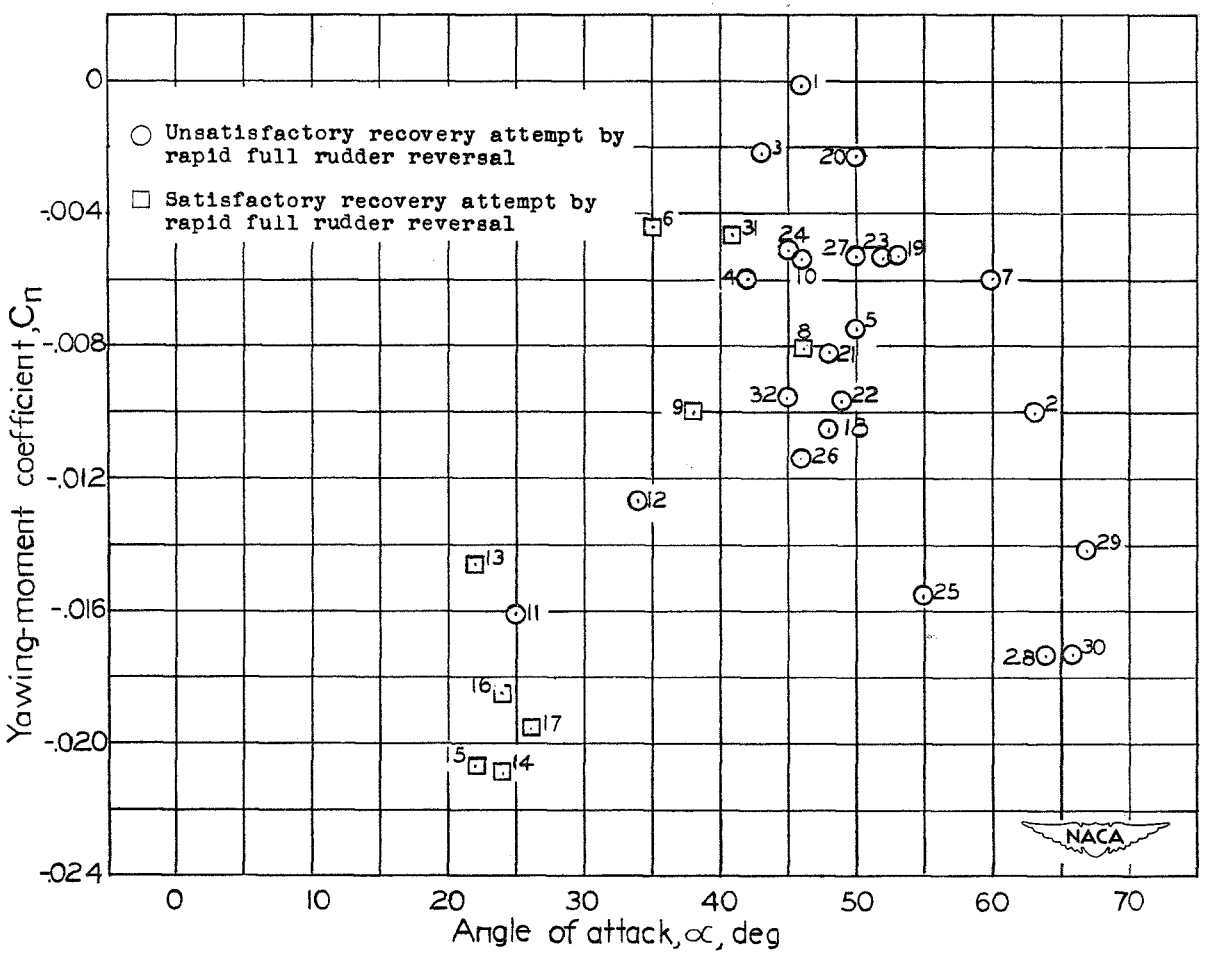

Figure 18.- Variation of yawing-moment coefficient caused by setting the rudder against the spin with angle of attack for spins of a model of a fighter airplane. Numbers refer to test conditions in table III.

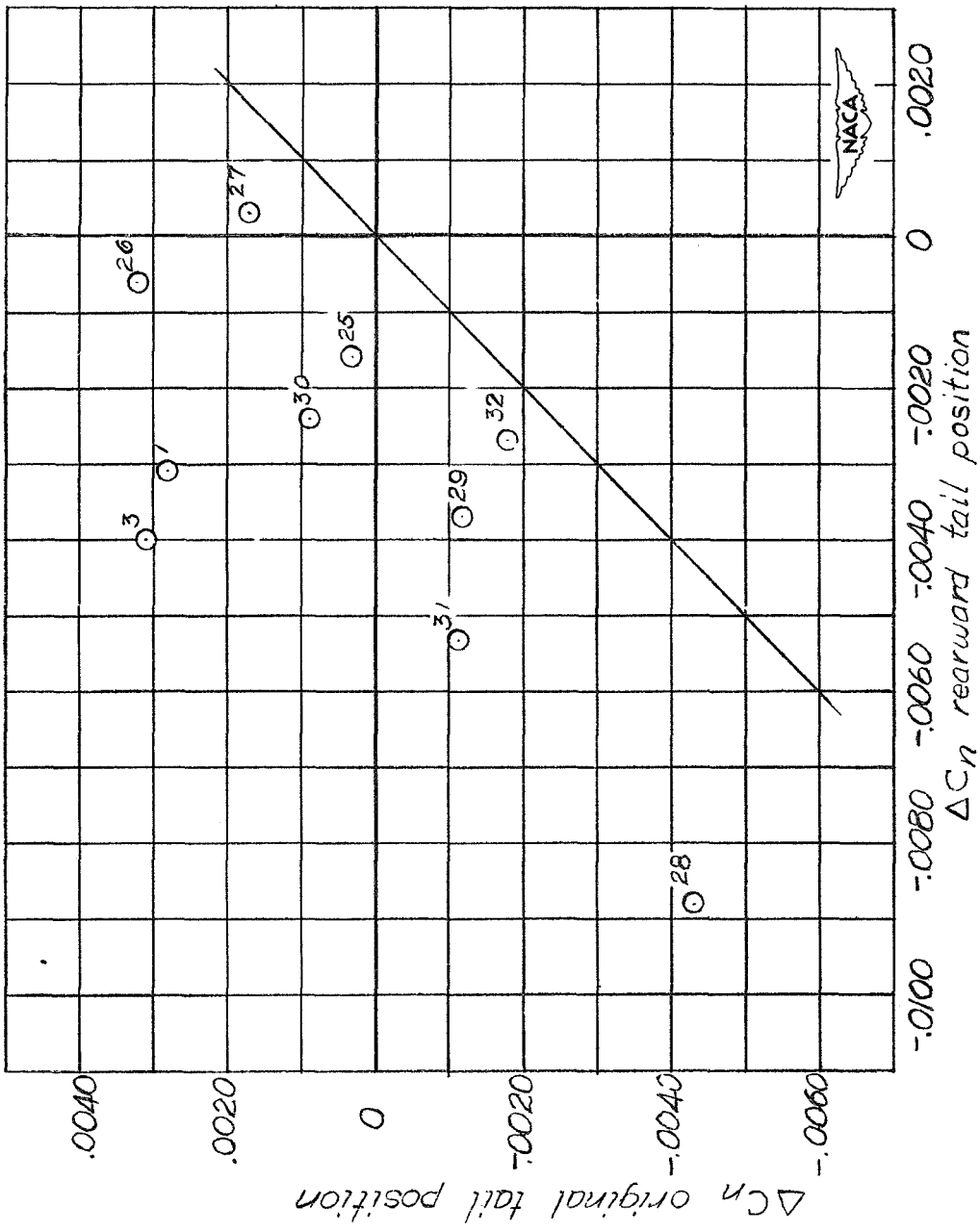

Figure 19.- Effect of horizontal-tail position on the increment of yawing-moment coefficient caused by rudder reversal for spins of a model of a fighter airplane. Numbers refer to test conditions in table III.

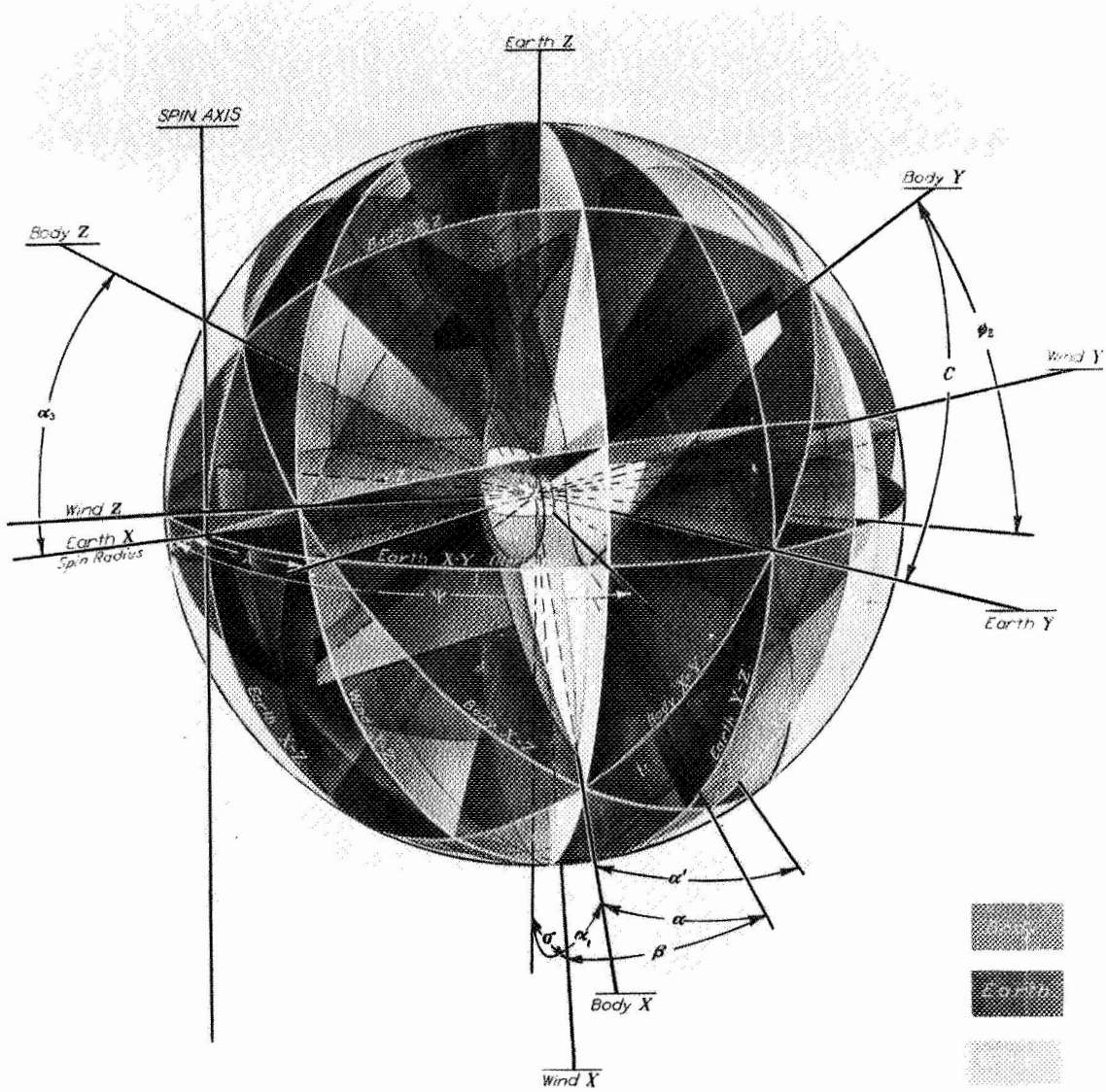

NACA

L-56398

Figure 20.- Illustration of several systems of axes with relation to a spinning airplane. Body, wind, and earth axes are shown.